Nonlinear Analysis: Hybrid Systems 52 (2024) 101472

Contents lists available at ScienceDirect

Nonlinear Analysis: Hybrid Systems

journal homepage: www.elsevier.com/locate/nahs

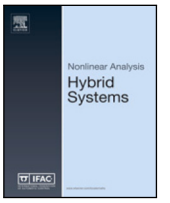

Saddle–node canard cycles in slow–fast planar piecewise linear differential systems

V. Carmona [a], S. Fernández-García [b], A.E. Teruel [c,*]

[a] Dpto. Matemática Aplicada II & IMUS, University of Seville, Escuela Superior de Ingenieros, Avenida de los Descubrimientos s/n, 41092 Sevilla, Spain
[b] Dpto. EDAN & IMUS, University of Seville, Facultad de Matemáticas, C/ Tarfia, s/n., 41012 Sevilla, Spain
[c] Departament de Matemàtiques i Informàtica & IAC3, Universitat de les Illes Balears, Palma de Mallorca, Spain

ARTICLE INFO

MSC:
primary 34C05
34C23
34C25
34E15
34E17
secondary 37G15
37G25

Keywords:
Piecewise linear systems
Bifurcations
Slow–fast differential systems
Canard orbits
Saddle–node canard orbits

ABSTRACT

By applying a singular perturbation approach, canard explosions exhibited by a general family of singularly perturbed planar Piecewise Linear (PWL) differential systems are analyzed. The performed study involves both hyperbolic and non-hyperbolic canard limit cycles appearing after both, a supercritical and a subcritical Hopf bifurcation. The obtained results are comparable with those obtained for smooth vector fields. In some sense, the manuscript can be understood as an extension towards the PWL framework of the results obtained for smooth systems by Dumortier and Roussarie in Mem. Am. Math. Soc. 1996, and Krupa and Szmolyan in J. Differ. Equ. 2001. In addition, some novel slow–fast behaviors are obtained. In particular, in the supercritical case, and under suitable conditions, it is proved that the limit cycles are organized along a curve exhibiting two folds. Each of these folds corresponds to a saddle–node bifurcation of canard limit cycles, one involving headless canard cycles, and the other involving canard cycles with head. This configuration also occurs in smooth systems with N-shaped fast nullcline. However, it has not been previously reported in the Van der Pol system. Our results provide justification for this observation.

1. Introduction

Planar slow–fast systems are differential systems involving two variables which evolve with very different time-scale. In fact, the ratio defining the time-scale separation of both variables is assumed to be as small as desired, and it is considered as the singular parameter. This different scales splits the phase plane into regions where the orbits evolve in a very different way. Specifically, close to the fast nullcline, the flow evolves slowly, while far from it, the flow evolves quickly. This fact has important dynamical consequences as for instance an increasing sensitivity of the dependence of the dynamics with respect to the variation of the parameters. One of the best known examples of this sensitivity is the so-called canard explosion where the amplitude of a small limit cycle increases very suddenly while a system parameter varies in an exponentially small range, see [1–3].

The canard explosion phenomenon was first described and analyzed by Benoit et al. in 1981 [4] in the Van der Pol oscillator, and explains the fast transition, by varying a parameter, from a small amplitude limit cycle born at a supercritical Hopf bifurcation, to a relaxation oscillation. Relaxation oscillations are oscillatory behavior characterized by long periods of quasi-static behavior interspersed with short periods of rapid transition. Since this behavior is usual in real-life phenomena, see [5] and references therein,

* Corresponding author.
E-mail address: antonioe.teruel@uib.es (A.E. Teruel).

https://doi.org/10.1016/j.nahs.2024.101472
Received 24 October 2023; Received in revised form 16 January 2024; Accepted 3 February 2024
Available online 8 February 2024
1751-570X/© 2024 The Authors. Published by Elsevier Ltd. This is an open access article under the CC BY license (http://creativecommons.org/licenses/by/4.0/).

models based in slow–fast differential equations are ubiquitous in many applications, such as chemical and biological ones, and in particular in neuroscience [6–8].

The main tools for the analysis of the slow–fast dynamics are provided by Geometric Singular Perturbation Theory [9], and rely on the ability of reconstructing the global dynamics by splitting and then joining, in a suitable way, the fast and slow behaviors. Under hyperbolicity conditions, Fenichel Theorems [10] describe the existence of invariant slow manifolds close to compact parts of the fast nullcline and also describe the stability properties of these slow manifolds. When the fast nullcline folds, normal hyperbolicity is usually lost at the fold, and Fenichel's theory does not apply. Instead, the system may exhibit canard dynamics (see [5]), involving peculiar trajectories that evolve close to the attracting branch of the slow manifold, pass near the folding point, and continue following the repelling branch of the slow manifold. Hence, in these systems, local aspects of the flow, as it is the local transition next the fold, can organize global dynamics.

A usual technique to analyze this local transition is the blow up of the fold [1,3,11]. Alternatively, some authors leverage the piecewise smooth context to analyze this transition within a simpler computational framework, while retaining all its salient features. Significant progress has been done in this sense. For instance, in the recent work [12] author analyzes relaxation oscillations in discontinuous piecewise smooth systems. Furthermore, in [13,14] the authors analyze the canard explosion in a continuous piecewise smooth context. Indeed, the simplest scenario in which this phenomenon can be replicated is within the piecewise linear (PWL) framework. Although certain dynamical aspects of slow–fast behavior had been observed in PWL systems (see [15–17] and references therein), understanding the proper replication of slow–fast dynamics in this context took some time (see [16,18,19]). In [20], the authors analyze a portion of the canard explosion phenomenon within the PWL context, specifically focusing on the explosion of hyperbolic headless canards.

In the present manuscript, we explore an extension of the system analyzed in [20], which allows for the coexistence of canard cycles, with and without head, as well as both hyperbolic and non-hyperbolic. Specifically, this extension involves replacing the fast U-shaped nullcline from the system in [20] with a fast N-shaped nullcline, represented by a four-segment polygonal curve. Three of these segments define the fold of the x-nullcline closer to the Hopf bifurcation point, maintaining the configuration and kink width of order $O(\sqrt{\varepsilon})$ as in [20], which allows for the existence of headless canard cycles. The fourth segment establishes a global return, facilitating the existence of canard cycles with head and relaxation cycles. This specific nullcline configuration has been shown to be effective in producing the canard explosion phenomenon. In fact, numerical evidence for a canard explosion in a PWL system with an equivalent nullcline configuration is presented in [17]. Conversely, approaches that do not take into account the third segment to mimic the fold only exhibit what has been termed the superexplosion phenomenon [19].

The results we obtain analytically prove the existence of a one parameter family of limit cycles starting at a Hopf-like bifurcation (both supercritical and subcritical) overcoming a canard explosion and ending at a relaxation oscillations. In addition, we give the limits of the canard regime and the critical value at which the connection between the attracting and repelling slow manifolds (maximal canard) occurs in terms of parameters. Our study allows for the analysis of the stability of the canard cycles. In particular, we obtain the existence and localization of saddle–node canard cycles. These results can be seen as an extension to the PWL context of the results obtained in the smooth context in [3].

Furthermore, we show new scenarios that, as far as we are aware, have not been previously reported in the smooth framework with cubic fast nullcline. In particular, we find situations where two saddle–node canard cycles along the same canard explosion take place: one saddle–node formed by the collapse of two headless canard cycles, and the other formed by the collapse of two canard cycles with head. As a consequence, we prove the coexistence of three canard limit cycles. This configuration already features in one of the simulation of PWL system showed in [17]. However, it is in the present work that a rigorous proof of its existence and of the essential geometric elements for its appearance is given. With consideration of this essential geometry, we are able to properly tune the Morris–Lecar neural model in order to exhibit two saddle–node canard cycles along the same canard explosion. This concludes that the presence of two saddle–node canard cycles is not exclusive of the PWL context.

The article is organized as follows. In Section 2, we provide a brief overview of canard explosion and saddle–node canard cycles in the smooth case. After that, in Section 3, we introduce the class of systems we aim to study. In Section 4, we present the main results of the paper. Section 5 is devoted to the proofs of the main results. Finally, Section 6 is devoted to conclusions and possible extensions of the present work. The technical issues of the proofs have been left to the Appendixes.

2. Background on canard cycles: canard explosion

In this section, based on [3,11], we briefly review the basic ingredients of the canard oscillatory behavior appearing in the smooth framework. Typically, canard solutions take place in planar differential systems of the form

$$\begin{cases} \varepsilon \dot{x} = f(x, y, a, \varepsilon), \\ \dot{y} = g(x, y, a, \varepsilon), \end{cases} \tag{1}$$

where $f, g \in C^r, r \geq 3$, $(x, y)^T \in \mathbb{R}^2$, $a \in \mathbb{R}$, $0 < \varepsilon \ll 1$ and the dot denotes the derivative with respect to the temporal variable τ. Since the norm of the derivative of solutions of system (1) is very different depending on the regions of the phase plane they are crossing through (far from the x-nullcline it is big and the solutions evolve very fast, and close to the x-nullcline it is small and the solutions evolve very slow), system (1) is often called *slow–fast system*.

After the rescaling in time $t = \tau/\varepsilon$, system (1) writes as

$$\begin{cases} x' = f(x, y, a, \varepsilon), \\ y' = \varepsilon g(x, y, a, \varepsilon), \end{cases} \tag{2}$$

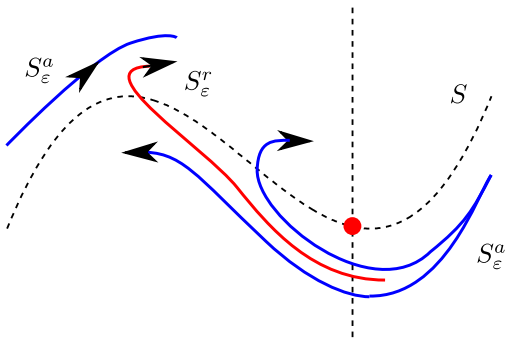

Fig. 1. Draft of the critical manifold S in the neighborhood of a canard point. An attracting branch S^a_ε, and a repelling branch S^r_ε, of the slow manifold obtained after singular perturbation are also represented. The canard cycles with and without head are obtained provided S^a_ε flows along one side or the other of a repelling manifold S^r_ε.

where the prime denotes the derivative with respect to the fast time t. Systems (1) and (2) are equivalent through the identity when $\varepsilon > 0$, but they have not the same limit for $\varepsilon = 0$. In fact, the limit of system (1), called *slow subsystem*, is a semi-explicit Differential Algebraic Equation (DAE), where the relation between the variables is given by

$$S = \{(x, y) : f(x, y, a, 0) = 0\}.$$

Assuming that $f_y(x, y, a, 0) \neq 0$, it follows that S is the graph of a differentiable function $y = \varphi_a(x)$, and the DAE reduces to the differential equation

$$f_x(x, \varphi_a(x), a, 0)\dot{x} = -f_y(x, \varphi_a(x), a, 0)g(x, \varphi_a(x), a, 0), \tag{3}$$

which is called the *reduced equation*. For a precise definition of the reduced flow we refer the reader to [5,9]. On the other hand, the limit for $\varepsilon = 0$ of system (2), called *fast subsystem*, is a differential equation having S as the locus of every equilibrium point. From here, S is called the *critical manifold*.

From Fenichel's Theorems [10,21], we obtain an approximation of the overall slow dynamics through the slow subsystem, and an approximation of the overall fast dynamics through the fast subsystem. In brief, Fenichel's theory asserts that compact subsets $S_0 \subset S$ formed by normally hyperbolic equilibrium points of the critical manifold, persist as locally invariant slow manifolds S_ε for $\varepsilon > 0$, which can be extended by the flow. Moreover, the stability properties of S_ε are equal to those of S_0. Furthermore, the flow over S_ε is a regular perturbation of the flow defined by the slow subsystem, or equivalently the reduced equation.

Typically, the breakdown of the normal hyperbolicity takes place at the points $(x_0, y_0) \in S$ where the manifold folds, i.e., $f_x(x_0, y_0, a, 0) = 0$ and $f_{xx}(x_0, y_0, a, 0) \neq 0$. It is possible to assume, without loss of generality, that the fold point is at the origin when $a = 0$, in that case we remove the sub-index at function φ_a, and therefore $\varphi(x) = \rho x^2 + O(x^3)$, with ρ a constant value different from 0. Hence, in a neighborhood of the origin two different branches of the critical manifold coexist, the attracting one, $S^a_0 = \{(x, y) : f_x(x, y, 0, 0) < 0\}$, and the repelling one, $S^r_0 = \{(x, y) : f_x(x, y, 0, 0) > 0\}$. Over each of these two branches the reduced Eq. (3) can be written as the ODE

$$\dot{x} = -\frac{f_y(x, \varphi(x), 0, 0)}{f_x(x, \varphi(x), 0, 0)} g(x, \varphi(x), 0, 0) = \frac{g(x, \varphi(x), 0, 0)}{\varphi'(x)},$$

and, assuming that $g(0, 0, 0, 0) \neq 0$, the flow defined by it has opposite orientation over each of these branches. In this case the fold point is called *jump point*.

A special situation occurs when the fold point at the origin satisfies that $g(0, 0, 0, 0) = 0$, together with the non-degeneracy condition $g_x(0, 0, 0, 0) \neq 0$. The reduced equation can be then regularized, defining a solution of the desingularized system which passes from one branch, S^a_0, to the other, S^r_0, through the fold point. In this case the fold point is called a *canard point*.

After perturbation, i.e., for $\varepsilon > 0$, Fenichel slow manifolds S^a_ε and S^r_ε behave in a different way near a jump fold point and near a canard point. Around a jump point, an attracting Fenichel slow manifold S^a_ε may follow closely the attracting branch S^a_0, pass in the vicinity of the fold point, and continue following approximately the fast dynamics, giving rise to the possibility of relaxation oscillations. However, around a canard point, a Fenichel slow manifold S^a_ε may follow closely the attracting branch of the critical manifold, S^a_0, pass in the vicinity of the fold point and then, surprisingly, continue following closely a repelling slow manifold S^r_ε, see Fig. 1. From this we can conclude the existence of solutions of the system (1) with $0 < \varepsilon \ll 1$ containing canard segments.

Under the existence of another attracting Fenichel slow manifold, see Fig. 1, when S^a_ε flows along one side or the other of the S^r_ε, there can exist *canards without head* or *canards with head*, respectively. Since slow manifolds are exponentially close to one another, the presence of exponentially small terms in the expansions in power series of ε of the slow manifolds implies that their respective position can change upon an exponentially small parameter variation. This phenomenon is known as the *canard explosion*. Moreover, the transition from canards without head to canards with head occurs typically when S^a_ε connects to S^r_ε. This connection takes place along a curve $a_S(\varepsilon)$ in the parameter plane (ε, a) and the associated canard solution is said to be a *maximal canard*.

Canard cycles develop along a branch born at a Hopf bifurcation, at $a = a_H$, and the canard explosion takes place around a value which is at a distance of $O(\varepsilon)$ from the a_H. This means that very close to the bifurcation point a_H, before the explosion, the cycles have the characteristics of typical Hopf cycles. This Hopf bifurcation arises only for $\varepsilon > 0$ and is usually known as a singular Hopf bifurcation [22,23].

The existence of saddle–node bifurcation of canard cycles in the smooth framework has been analyzed in [3]. There, the authors consider two different cases, depending whether the Hopf bifurcation where the cycle is born is supercritical or subcritical. Thus, after proving the existence of the maximal canard, they distinguish two different scenarios:

- *Supercritical case*: In Theorem 3.3, the authors state the existence of a family of periodic orbits. These periodic orbits can be stable Hopf-type limit cycles, canard limit cycles or relaxation oscillations. To analyze the stability of the canard limit cycles, they use the *way in-way out function* $R(s)$, which is the limit of the integral of the divergence along the slow manifolds when $\varepsilon \to 0$. In Theorem 3.4, assuming that this function is negative, the authors state that the canard limit cycles of the family are stable.
- *Subcritical case*: In Theorem 3.5, the authors state the existence of another family of periodic orbits. The orbits of that family can be unstable Hopf-type limit cycles, canard limit cycles or relaxation oscillations. Again, to analyze the stability of canard cycles, they use the *way in-way out function* $R(s)$. In Theorem 3.6, assuming that this function has exactly one simple zero at $s = s_{lp,0}$, the authors state that there exists a function $s_{lp}(\sqrt{\varepsilon})$ having limiting point at $s_{lp,0}$ when $\varepsilon \to 0$, such that canard limit cycles are unstable for $s < s_{lp}(\sqrt{\varepsilon})$ and stable for $s > s_{lp}(\sqrt{\varepsilon})$.

The concept of the way in-way out function $R(s)$ used in [3], derives from the idea of the slow divergence integral originally introduced in [1] and used among others, for instance, in [24].

3. The piecewise linear system: some preliminaries

In this section we introduce the family of PWL differential systems we are going to work with, together with some basic elements of their dynamics. We also define some functions and quantities which are needed for stating the main results in the next section.

Let us consider the following family of planar differential systems depending on the four-dimensional parameter $\boldsymbol{\kappa} = (a, k, \varepsilon, m)$,

$$\begin{cases} x' = y - f(x, a, k, \varepsilon, m), \\ y' = \varepsilon(a - x), \end{cases} \tag{4}$$

where the prime denotes the derivative with respect to the time t, $(x, y)^T \in \mathbb{R}^2$, $0 < \varepsilon \ll 1$, and the x-nullcline is defined by the graph of the continuous PWL function with four segments given by

$$f(x, a, k, \varepsilon, m) = \begin{cases} x + 1 - k(\sqrt{\varepsilon} - 1) - m(\sqrt{\varepsilon} + a), & \text{if } x < -1, \\ -k(x + \sqrt{\varepsilon}) - m(\sqrt{\varepsilon} + a), & \text{if } -1 < x \le -\sqrt{\varepsilon}, \\ m(x - a), & \text{if } |x| \le \sqrt{\varepsilon}, \\ x - \sqrt{\varepsilon} + m(\sqrt{\varepsilon} - a), & \text{if } x > \sqrt{\varepsilon}, \end{cases} \tag{5}$$

with $k > 2\sqrt{\varepsilon}$ and $|m| < 2\sqrt{\varepsilon}$.

Although the system looks like a piecewise linear version of the Van der Pol system (the x-nullcline profile is cubic-like, see Fig. 2, and the y-nullcline profile is a vertical straight line), the fact that in the central region we have a small slope m that can take different signs means that the change of stability of the equilibrium point produces a bifurcation that can be either supercritical or subcritical. Thus, although in appearance the system resembles a Van der Pol, in behavior it is closer to a FitzHugh–Nagumo, with the advantage that it has only one equilibrium point located at $x = a$. Since the slope of the outer segments of the x-nullcline is equal 1, the parameter k defines the relationship between the slope of the central segment and the slope of the outer ones.

We note that the three-segment fold in function f is considered here to allow for a proper canard dynamic around the fold [20], whereas the fourth segment is considered to allow for a global return that enables the existence of relaxation oscillations.

The PWL character of the vector field (4) allows the phase space to be divided into four regions: the lateral half-planes $\sigma_{LL} = \{(x, y) : x \le -1\}$ and $\sigma_R = \{(x, y) : x \ge \sqrt{\varepsilon}\}$, and the central bands $\sigma_L = \{(x, y) : -1 \le x \le -\sqrt{\varepsilon}\}$ and $\sigma_C = \{(x, y) : |x| \le \sqrt{\varepsilon}\}$, so that, restricted to these regions the vector field is linear and can be expressed in a matrix way as $F_i(\mathbf{x}) = A_i\mathbf{x} + \mathbf{b}_i$ with $i \in \{LL, L, C, R\}$, being

$$A_{LL} = \begin{pmatrix} -1 & 1 \\ -\varepsilon & 0 \end{pmatrix}, \; A_L = \begin{pmatrix} k & 1 \\ -\varepsilon & 0 \end{pmatrix}, \; A_C = \begin{pmatrix} -m & 1 \\ -\varepsilon & 0 \end{pmatrix}, \; A_R = \begin{pmatrix} -1 & 1 \\ -\varepsilon & 0 \end{pmatrix}, \tag{6}$$

$$\mathbf{b}_{LL} = \begin{pmatrix} (k + m)\sqrt{\varepsilon} + ma - (k + 1) \\ \varepsilon a \end{pmatrix}, \; \mathbf{b}_L = \begin{pmatrix} (k + m)\sqrt{\varepsilon} + ma \\ \varepsilon a \end{pmatrix}, \; \mathbf{b}_C = \begin{pmatrix} ma \\ \varepsilon a \end{pmatrix},$$

and

$$\mathbf{b}_R = \begin{pmatrix} \sqrt{\varepsilon}(1 - m) + ma \\ \varepsilon a \end{pmatrix}.$$

The local behavior of the flow of system (4) at any of the regions σ_i with $i \in \{LL, L, C, R\}$ is determined by the trace t_i, the determinant $d_i = \varepsilon$, the discriminant $\Delta_i = t_i^2 - 4\varepsilon$, the slow eigenvalue λ_i^s, the fast eigenvalue λ_i^q, the slow eigenvector $\mathbf{v}_i^s = (\lambda_i^s, -\varepsilon)^T$

Table 1
Significant quantities for the dynamics of system (4) in the lateral half-planes σ_{LL} and σ_R. Point $\mathbf{e}_i = -A_i^{-1}\mathbf{b}_i$ with $i \in \{LL, R\}$ is an equilibrium point only when $\mathbf{e}_{LL} \in \sigma_{LL}$ or $\mathbf{e}_R \in \sigma_R$.

	LL	R
t_i	-1	-1
Δ_i	$1-4\epsilon$	$1-4\epsilon$
λ_i^s	$\frac{-1+\sqrt{1-4\epsilon}}{2} = -\epsilon - \epsilon^2 + O(\epsilon^3)$	$\frac{-1+\sqrt{1-4\epsilon}}{2} = -\epsilon - \epsilon^2 + O(\epsilon^3)$
λ_i^q	$-1-\lambda_i^s$	$-1-\lambda_i^s$
$\mathbf{e}_i$	$\begin{pmatrix} a \\ 1+k-\sqrt{\epsilon}(m+k)-a(m-1) \end{pmatrix}$	$\begin{pmatrix} a \\ (m-1)(\sqrt{\epsilon}-a) \end{pmatrix}$

Table 2
Significant quantities for the dynamics of system (4) in the central bands σ_L and σ_C. Point $\mathbf{e}_i = -A_i^{-1}\mathbf{b}_i$ is an equilibrium point only when $\mathbf{e}_i$ is contained in its own region, that is, $\mathbf{e}_L \in \sigma_L$ or $\mathbf{e}_C \in \sigma_C$. There is no time-scale separation in the region σ_C because the eigenvalues there have the same modulus.

	L	C
t_i	k	$-m$
Δ_i	$k^2-4\epsilon$	$m^2-4\epsilon$
λ_i^s	$\frac{k-\sqrt{k^2-4\epsilon}}{2} = \frac{\epsilon}{k} + \frac{\epsilon^2}{k^3} + O(\epsilon^3)$	$-\frac{m}{2} \pm \frac{\sqrt{4\epsilon-m^2}}{2}\mathrm{i}$
λ_i^q	$k-\lambda_i^s$	
$\mathbf{e}_i$	$\begin{pmatrix} a \\ -(m+k)(\sqrt{\epsilon}+a) \end{pmatrix}$	$\begin{pmatrix} a \\ 0 \end{pmatrix}$

and the fast eigenvector $\mathbf{v}_i^q = (\lambda_i^q, -\epsilon)^T$ of the matrix A_i, and by the location of the point $\mathbf{e}_i = -A_i^{-1}\mathbf{b}_i$. We summarize all these significant quantities in Tables 1 and 2.

We remark that $\mathbf{e}_i$ are equilibrium points only when they are located in the region where the system (4) behaves as the linear system $\mathbf{F}_i(\mathbf{x}) = A_i\mathbf{x} + \mathbf{b}_i$.

From Lemma 4 in [25], the canonical slow manifold S_ϵ of system (4), with $0 < \epsilon \ll 1$, is locally formed by segments, each of them contained in a region σ_i with $i \in \{LL, L, R\}$ and defined by the slow eigenvector $\mathbf{v}_i^s = (\lambda_i^s, -\epsilon)^T$ associated to the slow eigenvalue λ_i^s. Hence,

$$S_\epsilon = \begin{cases} \mu_{LL} = \mathbf{e}_{LL} + r\mathbf{v}_{LL}^s & r \in \left[-\frac{1+a}{\lambda_{LL}^s}, +\infty\right), \\ \mu_L = \mathbf{e}_L - r\mathbf{v}_L^s & r \in \left[\frac{\sqrt{\epsilon}+a}{\lambda_L^s}, \frac{1+a}{\lambda_L^s}\right], \\ \mu_R = \mathbf{e}_R - r\mathbf{v}_R^s & r \in \left[\frac{a-\sqrt{\epsilon}}{\lambda_R^s}, +\infty\right). \end{cases} \tag{7}$$

Since $|m| < 2\sqrt{\epsilon}$, the matrix A_C has complex eigenvalues with modulus equal to $\sqrt{\epsilon}$, see Table 2. Therefore, in region σ_C there is not a real splitting between fast and slow behavior at the level of the eigenvalues. Consequently, there is no branch of the slow manifold contained in this region. On the contrary, the orbits flow along this region following in a completely regular way the continuation of the attracting branch of the slow manifold μ_R.

The region σ_C can be viewed as the domain where the Fenichel theory cannot be extended. In the smooth context, such a region is considered the blow up region, and has size $O(\sqrt{\epsilon})$, see Section 3.2 in [3]. From this, we fix the size of the central region in the definition of f to be $O(\sqrt{\epsilon})$, see (5), and consider the region σ_C as a blow-up of the corner appearing in the graph of f for $\epsilon = 0$.

We conclude that $S_\epsilon^a = \mu_{LL} \cup \mu_R$ and $S_\epsilon^r = \mu_L$ are the attracting branch and the repelling branch, respectively, of the canonical slow manifold S_ϵ. Moreover, the attracting branch S_ϵ^a intersects with the switching lines $\{x = -1\}$ and $\{x = \sqrt{\epsilon}\}$ at the points

$$\mathbf{q}_1^{LL} = \begin{pmatrix} -1 \\ -\lambda_{LL}^s(1+a) - k(\sqrt{\epsilon}-1) - m(\sqrt{\epsilon}+a) \end{pmatrix}, \quad \mathbf{q}_1^R = \begin{pmatrix} \sqrt{\epsilon} \\ (m+\lambda_R^s)(\sqrt{\epsilon}-a) \end{pmatrix}, \tag{8}$$

respectively, see Fig. 2, whereas the repelling branch S_ϵ^r intersects the switching lines $\{x = -1\}$ and $\{x = -\sqrt{\epsilon}\}$ at the points

$$\mathbf{q}_0^L = \begin{pmatrix} -\sqrt{\epsilon} \\ -(m+\lambda_L^s)(\sqrt{\epsilon}+a) \end{pmatrix}, \quad \mathbf{q}_1^L = \begin{pmatrix} -1 \\ -(m+k)(\sqrt{\epsilon}+a) + (1+a)\lambda_L^q \end{pmatrix}, \tag{9}$$

respectively. We also highlight the intersection points of the x-nullcline with the switching lines $\{x = -1\}, \{x = -\sqrt{\epsilon}\}$ and $\{x = \sqrt{\epsilon}\}$,

$$\mathbf{p}_{LL} = \begin{pmatrix} -1 \\ k(1-\sqrt{\epsilon}) - m(\sqrt{\epsilon}+a) \end{pmatrix}, \quad \mathbf{p}_L = \begin{pmatrix} -\sqrt{\epsilon} \\ -m(\sqrt{\epsilon}+a) \end{pmatrix}, \quad \mathbf{p}_R = \begin{pmatrix} \sqrt{\epsilon} \\ m(\sqrt{\epsilon}-a) \end{pmatrix}, \tag{10}$$

respectively. We note that except at these points, where the flow is tangent, the flow is transverse to the switch lines.

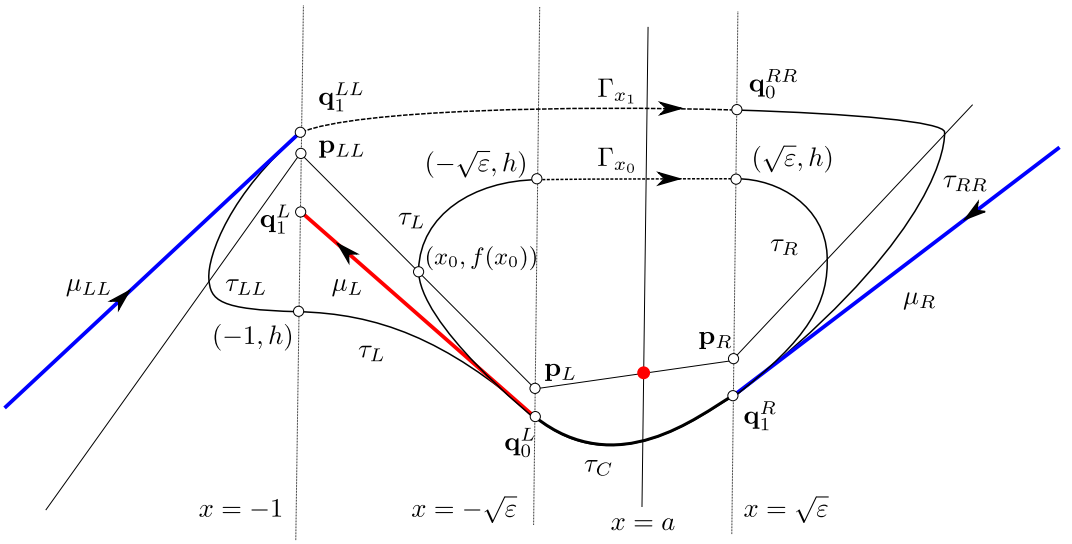

Fig. 2. Representation of the dynamical objects of system (4). Linearity regions $\sigma_{LL}, \sigma_L, \sigma_C$ and σ_R and switching lines $\{x = -1\}, \{x = -\sqrt{\varepsilon}\}$ and $\{x = \sqrt{\varepsilon}\}$. The fast nullcline given by the graph of the function $y = f(x, a, k, \varepsilon, m)$ and the intersection points with the switching lines $\mathbf{p}_{LL}, \mathbf{p}_L$ and $\mathbf{p}_R$. The slow nullcline $x = a$ and the equilibrium point at the intersection with the fast nullcline. Canonical slow manifold S_ε with the attracting branch $S_\varepsilon^a = \mu_{LL} \cup \mu_R$, the repelling branch $S_\varepsilon^r = \mu_L$, and the intersection points with the switching lines $\mathbf{q}_1^{LL}, \mathbf{q}_1^R$ and $\mathbf{q}_0^L, \mathbf{q}_1^L$, respectively. Headless canard limit cycle Γ_{x_0} with $x_0 \in (-1, -\sqrt{\varepsilon})$, canard limit cycle with head Γ_{x_1} with $x_1 < -1$, and maximal canard trajectory connecting the points $\mathbf{q}_1^R$ and $\mathbf{q}_0^L$.

Every limit cycle Γ of system (4) intersects the x-nullcline $(x, f(x, a, k, \varepsilon, m))$ at exactly one point $(x_\Gamma, f(x_\Gamma, a, k, \varepsilon, m))$ with $x_\Gamma < a$. We call *width of the limit cycle* Γ, to the first coordinate of this intersection point, that is x_Γ.

One special limit cycle, assuming that it exists, is the one having width $x_\Gamma = -1$. Such a limit cycle is tangent to the switching line $\{x = -1\}$ at the point $\mathbf{p}_{LL}$, and therefore, it is the separation cycle between the limit cycles intersecting the lateral region σ_{LL} and those that do not intersect it. In a similar way, the limit cycle having width $x_\Gamma = -\sqrt{\varepsilon}$ is tangent at $\mathbf{p}_L$ to the switching line $\{x = -\sqrt{\varepsilon}\}$ and it is the separation cycle between the limit cycles intersecting the region σ_L and those that do not intersect it.

When ε is small enough, canard limit cycles Γ with width $x_\Gamma > -1$ will be referred to as headless canard cycles, whereas canard limit cycles with width $x_\Gamma < -1$ will be referred to as canard cycles with head. Therefore, the limit cycle with width $x_\Gamma = -1$ will be referred as *the transitory canard*, see [26], and it is the boundary between headless canard cycles and canard cycles with head.

In addition, every limit cycle Γ where $x_\Gamma < -1$, intersects the separation line $\{x = -1\}$ at two points. Let $(-1, h)$ be the one below the point $\mathbf{p}_{LL}$, see Fig. 2. Moreover, every limit cycle, Γ with $x_\Gamma \in (-1, -\sqrt{\varepsilon})$, intersects the separation line $\{x = -\sqrt{\varepsilon}\}$ also at two points. Let $(-\sqrt{\varepsilon}, h)$ be the one over the point $\mathbf{p}_L$. We refer to h as the *height* of the limit cycle Γ.

Therefore, any limit cycle can be labeled by the two different quantities that we have denoted by the width and by the height. Let Φ be the piecewise function which maps the width x of a limit cycle into its height h, i.e.

$$h = \Phi(x) = \begin{cases} \Phi_{3z}(x) & \text{if } x \in [-1, -\sqrt{\varepsilon}), \\ \Phi_{4z}(x) & \text{if } x < -1, \end{cases} \tag{11}$$

where Φ_{3z} is defined by the flow of the linear system in the region σ_L, and Φ_{4z} is defined by the flow, backward in time, of the linear system in the region σ_{LL}. Therefore, through $h = \Phi(x)$ we can pass from the width x of a limit cycle Γ to its height h. Typically, the height h is more convenient for computational purposes, whereas the width x is more convenient for stating the results.

To analyze the stability of the canard limit cycles in the PWL framework, it is not possible to use the same approach that it is used in the smooth context, since the singularity of the reduced flow cannot be removed through the desingularization process [3]. In fact, the reduced Eq. (3) associated to the system (4) writes as

$$\dot{x} = \begin{cases} \frac{x}{k} & x < 0, \\ -x & x > 0, \end{cases}$$

where the equilibrium point at $x = 0$ persists after regularization. Therefore, the analysis of the stability of limit cycles through techniques based on the singular flow, such as the way-in/way-out function, [3,11], or the slow divergence integral, see [5,26] and references therein, cannot be successfully applied in this context. Nevertheless, this analysis can be performed directly when $\varepsilon > 0$ in the PWL context, by explicitly computing the integral of the divergence as the sum of the products of the traces of the linear systems and the time taken by the orbit to travel from one switching line to the next one (*time of flight*) along a region of linearity, see [27,28].

4. Statement of the main results

In this section we present the main results of the article. These results concern to the existence of a one parameter family of canard limit cycles in PWL system (4), and to the description about how this family organizes along a curve in the plane (x, a), where x is the width of the canard limit cycle and a is the parameter value. The results also provide information about the stability of the limit cycles, paying special attention to semi-stable ones. We note that, for simplicity, we limit all the following analysis to the values of the parameter $|m| < 2\sqrt{\varepsilon}$, given by $m = -\sqrt{\varepsilon}$ (for the supercritical case) and by $m = \sqrt{\varepsilon}$ (for the subcritical case). We suggest that the overall scenario $m = C\sqrt{\varepsilon}$ with $0 < |C| < 2$ would not substantially differ from the one presented here, except for the expressions appearing in the ensuing outcomes. Finally, we also note that in order to be fluid in the exposition, the proofs and their technical issues are left for next sections.

In the first result we assure that the starting point of the curve organizing the family of limit cycles exhibited by system (4) takes place at a Hopf-like bifurcation [28]. At this bifurcation, a limit cycle appears after the change of stability of the singular point, just like in the Hopf bifurcation. Nevertheless, in the Hopf-like bifurcation, the change of the stability occurs because the equilibrium point changes the region at which it is located. This results in differences between both bifurcations, particularly in the relationship between the amplitude of the limit cycle and the bifurcation parameter. Whereas in the Hopf-like bifurcation, it is linear, in the Hopf bifurcation, it is the square root.

The proof of the following result is a straightforward conclusion of Theorems 5.1 and 5.2 in [29], see also [28,30,31], and figures therein.

Theorem 4.1 (*Hopf-like Bifurcation*). *System (4) has a unique singular point* $\mathbf{e} = (a, f(a))$*, which converges to the corner of the critical manifold at the origin as* (ε, a) *tends to zero. Moreover, assume that* $m = \pm\sqrt{\varepsilon}$*, then the equilibrium changes its stability through a Hopf-like bifurcation as* a *passes through* $a = -m$*. In particular, when* $\varepsilon > 0$ *is sufficiently small, if* $m = -\sqrt{\varepsilon}$*, a stable limit cycle appears in a supercritical bifurcation when* $a < -m$*, and if* $m = \sqrt{\varepsilon}$*, an unstable limit cycle appears in a subcritical bifurcation when* $a > -m$*. In both cases, the amplitude of the limit cycle depends linearly on the distance* $|m + a|$.

Next theorem is devoted to the existence of a trajectory connecting the attracting branch and the repelling branch of the slow manifold. This connection is usually referred to as the *maximal canard* trajectory, see the piece of trajectory connecting the points $\mathbf{q}_1^R$ and $\mathbf{q}_0^L$ in Fig. 2.

Theorem 4.2 (*Maximal Canard Trajectory*). *Let us consider system (4) with* $m = s\sqrt{\varepsilon}$ *and* $s = \pm 1$*, and let* $\mathbf{q}_1^R$ *and* $\mathbf{q}_0^L$ *be the points given in (8) and (9), respectively. There exist a value* $0 < \mu \ll 1$ *and two analytic functions* A_S *and* η_S *defined in* $U = (0, +\infty) \times (-\mu, \mu)$ *such that, if* $0 < \varepsilon < \mu^2$ *and* $a = a_S(k, \varepsilon; m) := \sqrt{\varepsilon} A_S(k, \sqrt{\varepsilon}; s)$*, then the orbit of system (4) starting at the point* $\mathbf{q}_1^R$ *reaches the switching line* $\{x = -\sqrt{\varepsilon}\}$ *at the point* $\mathbf{q}_0^L$ *with the time of flight* $\tau_C^S(k, \varepsilon; m) := \eta_S(k, \sqrt{\varepsilon}; s)/\sqrt{\varepsilon} > 0$*. In addition, the first terms of the expansions of* a_S *and* τ_C^S *in terms of* $\sqrt{\varepsilon}$ *are given by*

$$a_S(k, \varepsilon; m) = -s\,\frac{e^{\frac{\pi}{\sqrt{3}}} - 1}{e^{\frac{\pi}{\sqrt{3}}} + 1}\sqrt{\varepsilon} - \frac{e^{\frac{\pi}{\sqrt{3}}}}{\left(e^{\frac{\pi}{\sqrt{3}}} + 1\right)^2}\left(\frac{1 - k^2}{k^2}\right)\varepsilon^{3/2} + O(\varepsilon^2) \tag{12}$$

and

$$\tau_C^S(k, \varepsilon; m) = \frac{2\pi}{\sqrt{3}}\frac{1}{\sqrt{\varepsilon}} - \frac{1 + k}{k} + s\,\frac{1 - k^2}{2k^2}\sqrt{\varepsilon} + O(\varepsilon). \tag{13}$$

The existence of the maximal canard trajectory, together with the divergence of the flow in a neighborhood of the canonical slow manifold, provide the arguments that we use in Section 5 to prove the following result about the existence of canard limit cycles, both with and without head (see Fig. 2), of any suitable width. To state the result in a proper way we introduce, by means of the function $a_S(k, \varepsilon; m)$ defined in Theorem 4.2, the following values

$$x_r = a_S - \frac{2(1 + a_S)}{1 + \varepsilon|\ln(\varepsilon)|}, \quad x_s = -\sqrt{\varepsilon} - \left(\left(1 + \frac{1}{|\ln\varepsilon|}\right)^{1/k} - 1\right)(\sqrt{\varepsilon} + a_S). \tag{14}$$

These values correspond with the end points of the interval such that limit cycles having width contained in (x_r, x_s) are canard limit cycles, see Lemma A.1. In fact, limit cycles having width $x < x_r$ are relaxation oscillations whereas limit cycles having width $x > x_s$ are still under the effect of the Hopf-like bifurcation.

Theorem 4.3 (*Existence of Canard Limit Cycles*). *Let us fix* $\varepsilon_0 > 0$ *sufficiently small and let us consider* $m = s\sqrt{\varepsilon}$ *with* $s = \pm 1$*, and* x_r *and* x_s *as given in (14) for* $\varepsilon \in (0, \varepsilon_0)$*. There exists a function* $a_N(k, \varepsilon, x_0; m)$*,* C^∞ *function of* $(k, \sqrt{\varepsilon}, x_0)$*, defined in the open set* $U = (0, +\infty) \times (0, \varepsilon_0) \times (x_r, x_s)$ *such that, for* $(k, \varepsilon, x_0) \in U$ *and* $a = a_N(k, \varepsilon, x_0; m)$ *system (4) possesses a canard limit cycle,* Γ_{x_0}*, passing through* $(x_0, f(x_0))$*. The canard limit cycle is headless if* $x_0 \in (-1, x_s)$ *and with head if* $x_0 \in (x_r, -1)$*. Moreover, the following relations*

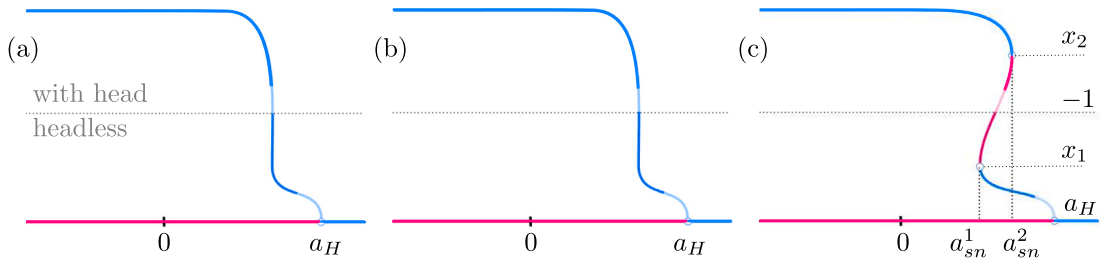

Fig. 3. Representation of the supercritical canard explosion. Width of limit cycles of system (4) versus the parameter a, in the supercritical case $m = -\sqrt{\varepsilon}$. The dotted line in all panels corresponds with the width of the transitory canard, i.e. the boundary between headless canard cycles and canard cycles with head. Moreover, shaded parts of the curves refer to the regions where the sign of the functions R_{3z} and R_{4z} do not guarantee the stability of the limit cycle. In panels (a) and (b) we represent the cases where $k < 1$ and $k = 1$, respectively. In these cases, the limit cycle appearing after the supercritical bifurcation at a_H exhibits a canard explosion. Panel (c) corresponds with the case $k > 1$. Here, two saddle nodes of width $x_1 < x_2$, take place at the values $a^1_{sn} < a^2_{sn}$ after the Hopf bifurcation at a_H.

hold

$$\begin{aligned} |a_N(k,\varepsilon,x_0;m) - a_S(k,\varepsilon;m)| &= O\left(|x_0 - a_S|^k e^{-\frac{|x_0-a_S|^k}{\varepsilon^{1+k/2}}}\right) \quad x_0 \in [-1, x_s), \\ |a_N(k,\varepsilon,x_0;m) - a_S(k,\varepsilon;m)| &= O\left(|x_0 + 1| e^{-\frac{k}{\varepsilon}\ln\left(\frac{1+a_S}{\sqrt{\varepsilon}+a_S}\right)}\right) \quad x_0 \in (x_r, -1), \end{aligned} \tag{15}$$

where the function a_S defined in Theorem 4.2.

The preceding result describes the canard explosion taking place in the PWL framework. There, it can be observed that the slope of the explosion is different before and after the transitory canard taking place at $x = -1$.

In the next result we establish the stability of the canard limit cycles obtained in the previous theorem. To do this, we compute a piecewise smooth function

$$R(x) = \begin{cases} R_{3z}(x) & x \in [-1, x_s), \\ R_{4z}(x) & x \in (x_r, x_u), \end{cases}$$

where

$$x_u = -1 - \left(\frac{1}{|\ln(\varepsilon)|} - \varepsilon\right)(1 + a_S), \tag{16}$$

(see Lemma A.1), a_S is defined in Theorem 4.2, and functions $R_{3z}(x)$ and $R_{4z}(x)$ are given in (28) and (30), respectively. The function R approximates the integral of the divergence along the limit cycle Γ_x, and uses the sign of this function to conclude the stability of Γ_x. Nevertheless, this approach does not produce accurate results if the canard limit cycle is close to the transitory canard, the one having width $x = -1$. The interval where the sign of $R(x)$ does not provide the stability of the canard limit cycles is given by $(x_u, -1)$. We organize the results into two theorems depending on whether the Hopf-like bifurcation is supercritical or subcritical. We illustrate the Theorems with Figs. 3 and 4.

Theorem 4.4. *Set $\varepsilon_0 > 0$ sufficiently small and let us consider $m = -\sqrt{\varepsilon}$, x_r and x_s as given in (14), x_u as given in (16) for $\varepsilon \in (0, \varepsilon_0)$ and $x_0 \in (x_r, x_u) \cup [-1, x_s)$. Take Γ_{x_0} the canard limit cycle of system (4) whose existence has been proved in Theorem 4.3 for the parameter value $a = a_N(k, \varepsilon, x_0; m)$. The following statements hold:*

(a) For $k \leq 1$, the canard limit cycle Γ_{x_0} is hyperbolic and stable.

(b) For $k > 1$ and $0 < \varepsilon < \varepsilon_0$ small enough, there exist exactly two values $x_1 \in (-1, x_s)$ and $x_2 \in (x_r, x_u)$ such that the canard limit cycle Γ_{x_0} is hyperbolic and stable if $x_0 \in (x_r, x_2) \cup (x_1, x_s)$, hyperbolic and unstable if $x_0 \in (x_2, x_u) \cup (-1, x_1)$, and a saddle–node canard cycle if $x_0 = x_1$ and $x_0 = x_2$.

Remark 4.5. From Theorem 4.4, it could be concluded that any canard cycle Γ_{x_0} loses its stability when the parameter k increases and passes $k = 1$. However, this is not the case; unstable canard orbits (those with x_0 in the interval (x_1, x_2)) appear only for fixed $k > 1$ and ε sufficiently small, i.e. less than a value that depends on the parameter k.

Theorem 4.6. *Set $\varepsilon_0 > 0$ small enough and let us consider $m = \sqrt{\varepsilon}$, x_r and x_s as given in (14), x_u as given in (16) for $\varepsilon \in (0, \varepsilon_0)$, and $x_0 \in (x_r, x_u) \cup [-1, x_s)$. Let Γ_{x_0} be the canard limit cycle of system (4) whose existence has been proved in Theorem 4.3 for the parameter value $a = a_N(k, \varepsilon, x_0; m)$. The following statements hold:*

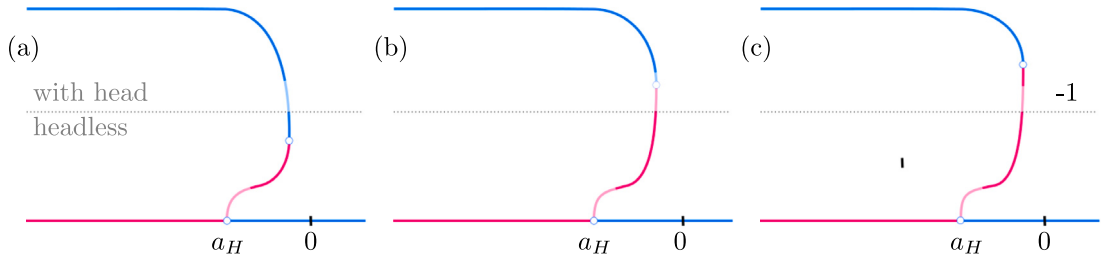

Fig. 4. Representation of the subcritical canard explosion. Width of limit cycles of system (4), versus the parameter a, in the subcritical case $m = \sqrt{\varepsilon}$. The dotted line in all panels corresponds with the transitory canard cycle with width $x = -1$. Moreover, shaded parts of the curves refer to the regions where the sign of the functions R_{3z} and R_{4z} do not guarantee the stability of the limit cycle. In panels (a) and (b) we represent the cases where $k < 1$ and $k = 1$, respectively, and in panel (c) we represent the case $k > 1$.

(a) For $k < 1$, there exists exactly one value $x_1 \in (-1, x_s)$ such that Γ_{x_0} is a hyperbolic limit cycle, if $x_0 \in (x_r, x_u) \cup (-1, x_s) \setminus \{x_1\}$, and a saddle–node canard cycle, if $x_0 = x_1$. Moreover, Γ_{x_0} is stable if $x_0 < x_1$ and unstable if $x_0 > x_1$.

(b) For $k = 1$, the canard limit cycle Γ_{x_0} is hyperbolic and stable if $x_0 \in (x_r, x_u)$ and hyperbolic and unstable if $x_0 \in (-1, x_s)$.

(c) For $k > 1$, there exists exactly one value $x_2 \in (x_r, x_u)$ such that Γ_{x_0} is hyperbolic, if $x_0 \in (x_r, x_u) \cup (-1, x_s) \setminus \{x_2\}$, and a saddle–node canard cycle, if $x_0 = x_2$. Moreover, Γ_{x_0} is stable if $x_0 < x_2$ and unstable if $x_0 > x_2$.

In the last main result, we state that for every width between the smallest canard cycle and the relaxation oscillation cycle, that is, for every $x_0 \in (x_r, x_u) \cup [-1, x_s)$, there exist values of the parameters such that system (4) exhibits a saddle–node canard limit cycle Γ_{x_0} of width x_0. We refer to Section 5.4 and Fig. 9 for a description of this result.

Theorem 4.7. *Set $\varepsilon_0 > 0$ small enough and let us consider $m = s\sqrt{\varepsilon}$ with $s = \pm 1$, x_r and x_s as given in (14), x_u as given in (16) for $\varepsilon \in (0, \varepsilon_0)$, and $x_0 \in (x_r, x_u) \cup [-1, x_s)$. There exist a value ε_1 and a function $k_{x_0}(\varepsilon)$ defined for $\varepsilon \in (0, \varepsilon_1)$, such that system (4) with parameters $k = k_{x_0}(\varepsilon)$ and $a = a_N(k_{x_0}(\varepsilon), \varepsilon, x_0; m)$ exhibits the saddle–node canard Γ_{x_0} whose existence has been stated in Theorem 4.4 for $m = -\sqrt{\varepsilon}$ and in Theorem 4.6 for $m = \sqrt{\varepsilon}$, respectively.*

5. Proofs of the main results

Let us begin by introducing some notation. For chosen parameters $\boldsymbol{\kappa} = (a, k, \varepsilon, m)$, and a point $\mathbf{p} \in \mathbb{R}^2$, we denote by

$$\varphi(t; \mathbf{p}, \boldsymbol{\kappa}) = (x(t; \mathbf{p}, \boldsymbol{\kappa}), y(t; \mathbf{p}, \boldsymbol{\kappa}))$$

the solution of system (4) with initial condition $\varphi(0; \mathbf{p}, \boldsymbol{\kappa}) = \mathbf{p}$. The coordinates of $\varphi(t; \mathbf{p}, \boldsymbol{\kappa})$ will be referred to as $x^i(t; \mathbf{p}, \boldsymbol{\kappa})$ and $y^i(t; \mathbf{p}, \boldsymbol{\kappa})$, with $i \in \{LL, L, C, R\}$, depending on the region where the solution belongs to, for that value of t.

First, we proceed to prove Theorem 4.2.

5.1. Proof of Theorem 4.2

The existence of the maximal canard solution reduces to the existence of an orbit connecting points $\mathbf{q}_1^R$ and $\mathbf{q}_0^L$, see Fig. 2. The set of conditions characterizing this connection is given by the existence of two values $\tau_C^S > 0$ and $a_S \in \mathbb{R}$, depending on k, $m = s\sqrt{\varepsilon}$ and ε such that the following conditions hold:

$$\begin{cases} F_1(\tau_C^S, a_S, k, \varepsilon; s) = 0, \\ F_2(\tau_C^S, a_S, k, \varepsilon; s) = 0, \\ F_1(t, a_S, k, \varepsilon; s) \in \left(0, 2\sqrt{\varepsilon}\right) \quad \text{for all} \quad t \in (0, \tau_C^S), \end{cases} \tag{17}$$

where $m = s\sqrt{\varepsilon}$, $s = \pm 1$, $0 < \varepsilon \ll 1$, $k > 0$, $|a_S| < \sqrt{\varepsilon}$, and the functions F_1 and F_2 are given by

$$\begin{cases} F_1(\tau, a, k, \varepsilon; s) = x^C(\tau; \mathbf{q}_1^R, a, k, \varepsilon, s) + \sqrt{\varepsilon}, \\ F_2(\tau, a, k, \varepsilon; s) = y^C(\tau; \mathbf{q}_1^R, a, k, \varepsilon, s) + (\lambda_L^s - \sqrt{\varepsilon})(\sqrt{\varepsilon} + a), \end{cases} \tag{18}$$

being x^C and y^C are the solution of the linear differential system defined in the central band σ_C, given by,

$$\begin{aligned}
&x^C(\tau;\mathbf{q}_1^R,a,k,\varepsilon,s)=\\
&\frac{e^{-s\frac{\sqrt{\varepsilon}}{2}\tau}(\sqrt{\varepsilon}-a)}{\sqrt{3}}\left(\left(\frac{2\lambda_R^s}{\sqrt{\varepsilon}}+s\right)\sin\left(\frac{\sqrt{3\varepsilon}}{2}\tau\right)+\sqrt{3}\cos\left(\frac{\sqrt{3\varepsilon}}{2}\tau\right)\right)+a,\\
&y^C(\tau;\mathbf{q}_1^R,a,k,\varepsilon,s)=\\
&\frac{e^{-s\frac{\sqrt{\varepsilon}}{2}\tau}(\sqrt{\varepsilon}-a)}{\sqrt{3}}\left(\left(\lambda_R^s+s\sqrt{\varepsilon}\right)\sqrt{3}\cos\left(\frac{\sqrt{3\varepsilon}}{2}\tau\right)+\left(s\,\lambda_R^s-\sqrt{\varepsilon}\right)\sin\left(\frac{\sqrt{3\varepsilon}}{2}\tau\right)\right).
\end{aligned}\tag{19}$$

The change of variables

$$(\tau,a,k,\varepsilon;s)=\left(\eta\delta^{-1},A\delta,k,\delta^2;s\right),\tag{20}$$

valid for $\varepsilon,\delta>0$, allows to write the system $F_1=0$ and $F_2=0$ into the equivalent form $\delta G_1(\eta,A,k,\delta;s)=0$ and $\delta^2 G_2(\eta,A,k,\delta;s)=0$, where G_1 and G_2 are given by

$$\begin{aligned}
&G_1(\eta,A,k,\delta;s)=\\
&3(A+1)+(A-1)e^{-s\eta/2}\left(-3\cos\left(\frac{\sqrt{3}\eta}{2}\right)+\frac{\sqrt{3}(-2s+5\delta)\sin\left(\frac{\sqrt{3}\eta}{2}\right)}{1-s\delta+\sqrt{1-4\delta^2}}\right),\\
&G_2(\eta,A,k,\delta;s)=\\
&\frac{3(1+A)(k+2s\delta)}{sk+2\delta+s\sqrt{k^2-4\delta^2}}+(A-1)e^{-s\eta/2}\left(\frac{3(-s+2\delta)\cos\left(\frac{\sqrt{3}\eta}{2}\right)}{1-2s\delta+\sqrt{1-4\delta^2}}+\frac{\sqrt{3}(s+2\delta)\sin\left(\frac{\sqrt{3}\eta}{2}\right)}{s+2\delta+s\sqrt{1-4\delta^2}}\right).
\end{aligned}$$

Since systems $(F_1,F_2)=(0,0)$ and

$$E_q(\eta,A,k,\delta;s):=(G_1(\eta,A,k,\delta;s),G_2(\eta,A,k,\delta;s))=(0,0),\tag{21}$$

are equivalent for $\delta=\sqrt{\varepsilon}>0$, from now on, we will find solutions for the second one.

From straightforward computations, it follows that the points

$$(\eta_0,A_0,k_0,\delta_0;s)=(2\pi/\sqrt{3},\mp(e^{\frac{\pi}{\sqrt{3}}}-1)/(e^{\frac{\pi}{\sqrt{3}}}+1),k,0;\pm1)$$

are solutions of system $(G_1,G_2)=(0,0)$. Since the partial derivatives in $(\eta_0,A_0,k_0,\delta_0;s)$ are

$$\begin{aligned}
&\frac{\partial G_1}{\partial\eta}=0,\quad \frac{\partial G_1}{\partial A}=3(1+e^{-s\frac{\pi}{\sqrt{3}}}),\\
&\frac{\partial G_2}{\partial\eta}=\frac{3}{1+e^{s\frac{\pi}{\sqrt{3}}}},\quad \frac{\partial G_2}{\partial A}=\frac{3}{2}\left(1+e^{-s\frac{\pi}{\sqrt{3}}}\right),
\end{aligned}$$

the determinant of the Jacobian matrix is

$$\begin{aligned}
\det(D_{\eta,A}G(\eta_0,A_0,k_0,\delta_0;s))&=\begin{vmatrix}\frac{\partial G_1}{\partial\eta}(\eta_0,A_0,k_0,\delta_0;s) & \frac{\partial G_1}{\partial A}(\eta_0,A_0,k_0,\delta_0;s)\\ \frac{\partial G_2}{\partial\eta}(\eta_0,A_0,k_0,\delta_0;s) & \frac{\partial G_2}{\partial A}(\eta_0,A_0,k_0,\delta_0;s)\end{vmatrix}=\\
&-9e^{-s\frac{\pi}{\sqrt{3}}}\neq0.
\end{aligned}\tag{22}$$

Thus, from the Implicit Function Theorem we conclude that there exist a value $\mu>0$ and functions $A_S(k,\delta;s)$ and $\eta_S(k,\delta;s)$, analytic as a function of (k,δ), respectively, defined in the open set $U=(0,+\infty)\times(-\mu,\mu)$ and such that $E_q(\eta_S(k,\delta;s),A_S(k,\delta;s),k,\delta;s)=(0,0)$.

Therefore, the existence of the functions τ_C^S and a_S are guaranteed by undoing the change of variable (20). Moreover, the lower order terms in $\sqrt{\varepsilon}$ of such a solution coincides with those in the expression (12)–(13). The remainder terms in this approximated solution can be obtained by the method of the undetermined coefficients.

Finally, since the angle traveled by the solution from $\mathbf{q}_1^R$ to $\mathbf{q}_0^L$ satisfies that $\sqrt{3\varepsilon}\tau_C^S(k,\varepsilon;m)/2<\pi$, and $|a_S(k,\varepsilon;m)|<\sqrt{\varepsilon}$, it follows that the inequality in third expression in (17) is fulfilled. Therefore, we conclude that for $a=a_S(k,\varepsilon;m)$ system (4) exhibits an orbit connecting the slow manifolds with time of flight equal to $\tau_C^S(k,\varepsilon;m)>0$.

Next, we provide the proof of Theorem 4.3.

5.2. Proof of Theorem 4.3

We begin with the proof for the headless canard limit cycles. Consider a point $(x_0, f(x_0))$ with $x_0 \in (-1, x_s)$, and the orbit Γ_{x_0} through this point, see Fig. 2. By integrating both forward and backward in time, the orbit targets the switching line $\{x = -\sqrt{\varepsilon}\}$ at two points, respectively,

$$\begin{pmatrix} -\sqrt{\varepsilon} \\ h \end{pmatrix}, \qquad \mathbf{p}_0 = \mathbf{q}_0^L + \begin{pmatrix} 0 \\ he^{-\frac{kh}{\varepsilon(\sqrt{\varepsilon}-a)}} \end{pmatrix}.$$

The expression of $\mathbf{p}_0$ follows from Lemma A.2, since $h = \Phi_{3z}(x_0) > h_s$ provided that $x_0 \in (-1, x_s)$, see Lemma A.1. Moreover, Γ_{x_0} also intersects forward in time the switching line $\{x = \sqrt{\varepsilon}\}$ at the two points

$$\mathbf{p} = \begin{pmatrix} \sqrt{\varepsilon} \\ h + O(\varepsilon^2) \end{pmatrix}, \qquad \mathbf{p}_1 = \mathbf{q}_1^R + \begin{pmatrix} 0 \\ (h + O(\varepsilon^2))e^{-\frac{h}{\varepsilon(\sqrt{\varepsilon}-a)}} \end{pmatrix},$$

where the expression of $\mathbf{p}_1$ follows from Lemma A.2. The ordinate of the previous point $\mathbf{p}$ follows by taking into account that the y-coordinate of the solutions increases while $x \in (-\sqrt{\varepsilon}, a)$ and decreases while $x \in (a, \sqrt{\varepsilon})$.

The conditions for Γ_{x_0} to be a limit cycle require the existence of parameter values $\boldsymbol{\kappa} = (a, k, \varepsilon, m)$ such that the solution of the linear system in the central band σ_C, with an initial condition at $\mathbf{p}_1$, reaches the switching line $x = -\sqrt{\varepsilon}$ at point $\mathbf{p}_0$ for the first time. In other words, $e^{\tau A_C}(\mathbf{p}_1 - \mathbf{e}_C) + \mathbf{e}_C - \mathbf{p}_0 = \mathbf{0}$, where $\beta\tau < \pi$, with A_C being the matrix defined in (6), and β representing the imaginary part of the complex eigenvalue of A_C. By substituting the values of $\mathbf{p}_0$ and $\mathbf{p}_1$, the previous equation writes as

$$e^{\tau A_C}(\mathbf{q}_1^R - \mathbf{e}_C) + \mathbf{e}_C - \mathbf{q}_0^L + e^{\tau A_C}\begin{pmatrix} 0 \\ (h + O(\varepsilon^2))e^{-\frac{h}{\varepsilon(\sqrt{\varepsilon}-a)}} \end{pmatrix} - \begin{pmatrix} 0 \\ he^{-\frac{kh}{\varepsilon(\sqrt{\varepsilon}-a)}} \end{pmatrix} = \mathbf{0}. \tag{23}$$

Performing the change of variables given in (20) and multiplying by the matrix

$$M_\delta = \begin{pmatrix} \frac{1}{\delta} & 0 \\ 0 & \frac{1}{\delta^2} \end{pmatrix},$$

we obtain that expression (23) writes as $E_p(\eta, A, k, \delta, h; s) = \mathbf{0}$, where

$$E_p(\eta, A, k, \delta, h; s) = E_q(\eta, A, k, \delta; s) + M_\delta\left(e^{\eta B}\begin{pmatrix} 0 \\ (h + O(\delta))e^{-\frac{h}{\delta^3(1-A)}} \end{pmatrix} - \begin{pmatrix} 0 \\ he^{-\frac{kh}{\delta^3(1-A)}} \end{pmatrix}\right), \tag{24}$$

matrix B is given by

$$B = \begin{pmatrix} s & \frac{1}{\delta} \\ -\delta & 0 \end{pmatrix},$$

with $s = \operatorname{sign}(m)$, and $E_q(\eta, A, k, \delta; s)$ is the function given in (21) whose zeroes provide the connection between $\mathbf{q}_1^R$ and $\mathbf{q}_0^L$. Then, the Jacobian matrix respect to the variables η and A satisfies

$$D_{\eta,A}E_p\big|_{(\eta,A,k,\delta,h;s)} = D_{\eta,A}E_q\big|_{(\eta,A,k,\delta;s)} + M_\delta\left(e^{\eta B}\begin{pmatrix} (h + O(\delta))e^{-\frac{h}{\delta^3(1-A)}} & 0 \\ 0 & -\frac{(h^2+O(\delta))e^{-\frac{h}{\delta^3(1-A)}}}{\delta^3(1-A)^2} \end{pmatrix} - \begin{pmatrix} 0 & 0 \\ 0 & -\frac{kh^2e^{-\frac{kh}{\delta^3(1-A)}}}{\delta^3(1-A)^2} \end{pmatrix}\right).$$

Notice that

$$e^{\eta B} = e^{\alpha\eta}\begin{pmatrix} -\frac{\sin(\beta\eta)-\sqrt{3}\cos(\beta\eta)}{\sqrt{3}} & \frac{2\sin(\beta\eta)}{\sqrt{3}\delta} \\ -\frac{2\sin(\beta\eta)\delta}{\sqrt{3}} & \frac{\sin(\beta\eta)+\sqrt{3}\cos(\beta\eta)}{\sqrt{3}} \end{pmatrix},$$

where $\alpha = -\frac{s}{2}$ and $\beta = \frac{\sqrt{3}}{2}$. Hence, for every h with $h > O(\delta^3)$, the expression (24) can be extended to $\delta = 0$, and we conclude that $E_p(\eta, A, k, 0, h; s) = E_q(\eta, A, k, 0; s)$ and $D_{\eta,A}E_p\big|_{(\eta,A,k,0,h;s)} = D_{\eta,A}E_q\big|_{(\eta,A,k,0;s)}$.

From the proof of Theorem 4.2, it follows that

$$E_p(2\pi/\sqrt{3}, \mp(e^{\frac{\pi}{\sqrt{3}}} - 1)/(e^{\frac{\pi}{\sqrt{3}}} + 1), k, 0, h; \pm 1) = \mathbf{0},$$
$$\det\left(D_{\eta,A}E_p\big|_{(2\pi/\sqrt{3}, \mp(e^{\frac{\pi}{\sqrt{3}}}-1)/(e^{\frac{\pi}{\sqrt{3}}}+1), k, 0, h; \pm 1)}\right) = -9e^{\mp\frac{\pi}{\sqrt{3}}}.$$

Thus, we can apply the Implicit Function Theorem to the set of equations $E_p(\eta, A, k, \delta, h; s) = \mathbf{0}$, whose solutions provide the connection between $\mathbf{p}_1$ and $\mathbf{p}_0$, and conclude the existence of the functions $\eta = \eta_H(k, \delta, h; s)$ and $A = A_H(k, \delta, h; s)$ satisfying

$$E_p(\eta_H(k, \delta, h; s), A_H(k, \delta, h; s), k, \delta, h; s) = \mathbf{0}.$$

Furthermore, from the Mean Value Theorem in integral form for functions in several variables [32], it follows that

$$E_p(\eta_H(k,\delta,h;s), A_H(k,\delta,h;s), k,\delta,h;s) - E_p(\eta_S(k,\delta;s), A_S(k,\delta;s), k,\delta,h;s) = \tilde{E}_p(\eta_H, A_H, \eta_S, A_S, k,\delta,h;s)\begin{pmatrix}\eta_H(k,\delta,h;s)-\eta_S(k,\delta;s)\\ A_H(k,\delta,h;s)-A_S(k,\delta;s)\end{pmatrix},$$

where

$$\tilde{E}_p(\eta_H, A_H, \eta_S, A_S, k,\delta,h;s) = \int_0^1 D_{\eta,A}E_p(s\ \eta_H + (1-s)\eta_S, s\ A_H + (1-s)A_S, k,\delta,h;s)\,ds.$$

Applying now Eq. (24), for δ small enough, it follows

$$-M_\delta\left(e^{\eta_S B}\begin{pmatrix}0\\ (h+O(\delta))e^{-\frac{h}{\delta^3(1-A_S)}}\end{pmatrix} - \begin{pmatrix}0\\ he^{-\frac{kh}{\delta^3(1-A_S)}}\end{pmatrix}\right) \approx \begin{pmatrix}0 & 3\left(1+e^{\frac{\pi}{\sqrt{3}}}\right)\\ \frac{2e^{\frac{\pi}{\sqrt{3}}}}{1+e^{\frac{\pi}{\sqrt{3}}}} & -1-e^{\frac{\pi}{\sqrt{3}}}\end{pmatrix}\begin{pmatrix}\eta_H(k,\delta,h;s)-\eta_S(k,\delta;s)\\ A_H(k,\delta,h;s)-A_S(k,\delta;s)\end{pmatrix}.$$

Hence,

$$\begin{pmatrix}\eta_H(k,\delta,h;s)-\eta_S(k,\delta;s)\\ A_H(k,\delta,h;s)-A_S(k,\delta;s)\end{pmatrix} \approx -\begin{pmatrix}\frac{1+e^{-\frac{\pi}{\sqrt{3}}}}{6\delta} & \frac{1+e^{-\frac{\pi}{\sqrt{3}}}}{2\delta^2}\\ \frac{1}{3\delta\left(1+e^{\frac{\pi}{\sqrt{3}}}\right)} & 0\end{pmatrix}\left(e^{\eta_S B}\begin{pmatrix}0\\ he^{-\frac{h}{\delta^3(1-A_S)}}\end{pmatrix} - \begin{pmatrix}0\\ he^{-\frac{kh}{\delta^3(1-A_S)}}\end{pmatrix}\right).$$

Isolating the second coordinates in the equality above, we conclude that

$$A_H(k,\delta,h;s) - A_S(k,\delta;s) \approx \frac{2\sin(\beta\eta_S)e^{\alpha\eta_S}}{3\sqrt{3}\delta^2\left(1+e^{\frac{\pi}{\sqrt{3}}}\right)}he^{-\frac{h}{\delta^3(1-A_S)}},$$

and then by undoing the change of variables we obtain

$$a_H(k,\varepsilon,h;m) - a_S(k,\varepsilon;m) = O\left(\frac{h}{\sqrt{\varepsilon}}e^{-\frac{h}{\varepsilon^{3/2}}}\right). \tag{25}$$

Finally, we consider the change of variables from h to the first component of the intersection of the orbit with the $x-$nullcline, x_0. To do this change, let $\varphi(t)$ be a solution of system (4) such that $\varphi(t) \subset \sigma_L$ for $t \in (0,t_0)$ and $t_0 > 0$. By using the Krylov base $\{\mathbf{p}_L, \dot{\mathbf{p}}_L\}$, the solution can be parametrized by $\varphi(t) = u_1(t)\mathbf{p}_L + u_2(t)\dot{\mathbf{p}}_L$. Following Theorem 5 in [33], function $H_L(u_1,u_2) = |u_1+\lambda_L^s u_2|^{\lambda_L^q}|u_1+\lambda_L^q u_2|^{-\lambda_L^s}$ is constant over the coordinates $(u_1(t),u_2(t))$ with $t \in (0,t_0)$, and it is called a first integral for system (4) related to the Krylov base $\{\mathbf{p}_L, \dot{\mathbf{p}}_L\}$. Therefore, the transition map from points on the $x-$nullcline in zone σ_L to points on the switching line $\{x = -\sqrt{\varepsilon}\}$, is given by

$$H_L(u,0) = H_L(1,v). \tag{26}$$

Now, we have

$$\begin{pmatrix}x_0\\ f(x_0)\end{pmatrix} = \mathbf{e}_L + u(\mathbf{p}_L - \mathbf{e}_L), \quad \begin{pmatrix}-\sqrt{\varepsilon}\\ h\end{pmatrix} = \mathbf{p}_L + v\dot{\mathbf{p}}_L,$$

from where we obtain,

$$u = \frac{a-x_0}{a+\sqrt{\varepsilon}}, \quad v = \frac{1}{\varepsilon}\left(\frac{h}{\sqrt{\varepsilon}+a}+m\right).$$

By substituting these expressions of u and v in (26) and taking into account that $u^k \approx \varepsilon v + 1$ (see function F in expression (26) in [30]), we deduce that,

$$h = \left(\left(\frac{a-x_0}{a+\sqrt{\varepsilon}}\right)^k - (1+m)\right)(a+\sqrt{\varepsilon}).$$

Finally, by substituting this expression in (25), we obtain the first expression in (15).

Let us continue with the proof in the case of a canard cycle Γ_{x_0} with head, that is $x_0 \in (x_r,-1)$. Starting at the point $(x_0, f(x_0))$ and integrating in backward time, the orbit targets the switching lines $\{x=-1\}$ and $\{x=-\sqrt{\varepsilon}\}$ at

$$\begin{pmatrix}-1\\ h\end{pmatrix} \quad \text{and} \quad \mathbf{p}_0 = \mathbf{q}_0^L - \begin{pmatrix}0\\ (k-h)e^{-\frac{k}{\varepsilon}\ln\left(\frac{1+a}{\sqrt{\varepsilon}-a}\right)}\end{pmatrix},$$

respectively, where the expression of $\mathbf{p}_0$ follows from Lemma A.2. Moreover, integrating forward in time, the orbit targets the switching line $\{x = \sqrt{\varepsilon}\}$ at two points

$$\begin{pmatrix} \sqrt{\varepsilon} \\ \bar{h} \end{pmatrix} \qquad \text{and} \qquad \mathbf{p}_1 = \mathbf{q}_1^R + \begin{pmatrix} 0 \\ \bar{h}e^{-\frac{\bar{h}}{\varepsilon(\sqrt{\varepsilon}-a)}} \end{pmatrix},$$

where the expression of $\mathbf{p}_1$ follows from Lemma A.2, and the constant $\bar{h}$ satisfies that $k + O(\sqrt{\varepsilon}) \leq \bar{h} \leq 1 + k + O(\sqrt{\varepsilon})$. These bounds for the value of $\bar{h}$ follows by taking into account that the y-coordinate of the solutions increases while $x \in (-1, a)$ and decreases while $x \in (a, \sqrt{\varepsilon})$.

The conditions for Γ_{x_0} to be a limit cycle require the existence of parameter values $\boldsymbol{\kappa} = (a, k, \varepsilon, m)$ such that the solution of the linear system in the central band σ_C, with an initial condition at $\mathbf{p}_1$, reaches the switching line $x = -\sqrt{\varepsilon}$ at point $\mathbf{p}_0$ for the first time. In other words, equation $e^{\tau A_C}(\mathbf{p}_1 - \mathbf{e}_C) + \mathbf{e}_C - \mathbf{p}_0 = \mathbf{0}$ has to be satisfied. This equation can be written in a similar way as (23). From here on, the proof follows in analogous way.

5.3. Proofs of Theorems 4.4 and 4.6

This subsection is devoted to the proof of Theorems 4.4 and 4.6. The outline of the proof is the following: First, we study the hyperbolicity/non-hyperbolicity of headless canard cycles. Second, we analyze the hyperbolicity/non-hyperbolicity of canard cycles with head. Finally, by proving a non-degeneracy condition on the derivative of the Poincaré map around the non-hyperbolic canard cycles, we prove the correspondence of non-hyperbolic canard cycles to saddle–node bifurcations.

5.3.1. Hyperbolicity/non-hyperbolicity of headless canard cycles

Let us begin by defining the Poincaré map in the neighborhood of periodic orbits visiting zones σ_L, σ_C and σ_R. Consider a point $\mathbf{p}_0 = (\sqrt{\varepsilon}, y_0)$ in the switching line $\{x = \sqrt{\varepsilon}\}$ and located between $\mathbf{p}_R$ and $\mathbf{q}_R^1$, see Fig. 2. From expressions (8) and (10) it follows that $(m + \lambda_R^s)(\sqrt{\varepsilon} - a) < y_0 < m(\sqrt{\varepsilon} - a)$. Assume now that there exists a time of flight $\tau_{Cd} > 0$ such that $x^C(\tau_{Cd}; \mathbf{p}_0, \boldsymbol{\kappa}) = -\sqrt{\varepsilon}$ and $x^C(t; \mathbf{p}_0, \boldsymbol{\kappa}) \in (-\sqrt{\varepsilon}, \sqrt{\varepsilon})$ for all $t \in (0, \tau_{Cd})$, where $x^C(t; \mathbf{p}_0, \boldsymbol{\kappa})$ is the first coordinate of the solution through $\mathbf{p}_0$ reduced to the central region σ_C, see (19). In such a case, we can define the Poincaré half-map between the switching lines $\{x = \sqrt{\varepsilon}\}$ and $\{x = -\sqrt{\varepsilon}\}$ at the point y_0 as $\Pi_{C_d}(y_0, \boldsymbol{\kappa}) = y^C(\tau_{Cd}; \mathbf{p}_0, \boldsymbol{\kappa})$. Similarly, we can define the Poincaré half-map between the switching lines $\{x = -\sqrt{\varepsilon}\}$ and $\{x = \sqrt{\varepsilon}\}$ at a point $y_2 > -m(\sqrt{\varepsilon} + a)$ as $\Pi_{C_u}(y_2, \boldsymbol{\kappa}) = y^C\left(\tau_{C_u}; \mathbf{p}_2, \boldsymbol{\kappa}\right)$, where $\tau_{C_u} > 0$ is the time of flight and $\mathbf{p}_2 = (-\sqrt{\varepsilon}, y_2)$.

Consider now a point $\mathbf{p}_1 = (-\sqrt{\varepsilon}, y_1)$ in the switching line $\{x = -\sqrt{\varepsilon}\}$ and located between $\mathbf{q}_L^0$ and $\mathbf{p}_L$, that is, $y_1 \in \left(-(m + \lambda_L^s)(\sqrt{\varepsilon} + a), -m(\sqrt{\varepsilon} + a)\right)$. Assume that there exists a time of flight $\tau_L > 0$ such that $x^L(\tau_L; \mathbf{p}_1, \boldsymbol{\kappa}) = -\sqrt{\varepsilon}$ and $x^L(t; \mathbf{p}_1, \boldsymbol{\kappa}) \in (-1, -\sqrt{\varepsilon})$ for all $t \in (0, \tau_L)$. Here $x^L(\tau_L; \mathbf{p}_1, \boldsymbol{\kappa})$ is the first coordinate of the solution through $\mathbf{p}_1$ and reduced to the region L. In such a case, we can define the Poincaré half-map between the switching line $\{x = -\sqrt{\varepsilon}\}$ and itself at the point y_1 as $\Pi_L(y_1, \boldsymbol{\kappa}) = y^L\left(\tau_L; \mathbf{p}_1, \boldsymbol{\kappa}\right)$. Similarly, we can define the Poincaré half-map between the switching line $\{x = \sqrt{\varepsilon}\}$ and itself at the point $y_3 > m(\sqrt{\varepsilon} - a)$ as $\Pi_R(y_3, \boldsymbol{\kappa}) = y^R\left(\tau_R; \mathbf{p}_3, \boldsymbol{\kappa}\right)$, where $\tau_R > 0$ is the time of flight and $\mathbf{p}_3 = (\sqrt{\varepsilon}, y_3)$. Expressions for Π_L^{-1} and Π_R can be found in Lemma A.2.

At this point, the Poincaré map for an orbit of system (4) visiting zones σ_L, σ_C and σ_R can be defined.

Definition 5.1. The Poincaré map Π in the neighborhood of an orbit Γ_{x_0} of system (4) visiting zones σ_L, σ_C and σ_R is defined as

$$\Pi(y_0, \boldsymbol{\kappa}) = \Pi_R(\Pi_{C_u}(\Pi_L(\Pi_{C_d}(y_0, \boldsymbol{\kappa}), \boldsymbol{\kappa}), \boldsymbol{\kappa}), \boldsymbol{\kappa}),$$

provided the composition of Poincaré half-maps is possible, where $y_0 = \Pi_{Cd}^{-1}(\Pi_L^{-1}(\Phi_{3z}(x_0), \boldsymbol{\kappa}), \boldsymbol{\kappa})$.

For ε fixed and small enough, suppose the existence of a headless canard limit cycle Γ_{x_0}, see Fig. 2, obtained under the parameter relation $a = a_N(k, \varepsilon, x_0; m)$ given in Theorem 4.3. The cycle Γ_{x_0} corresponds to the fixed point of the Poincaré map $\Pi(y_0, \boldsymbol{\eta})$, where $y_0 = \Pi_{Cd}^{-1}(\Pi_L^{-1}(\Phi_{3z}(x_0), \boldsymbol{\kappa}), \boldsymbol{\kappa})$.

To take into account the non-hyperbolicity of the canard cycle Γ_{x_0}, we consider the derivative of the Poincaré map, which corresponds to the exponential of the integral of the divergence of the system along Γ_{x_0}, see [27]. In the particular case of PWL systems, the integral of the divergence can be explicitly computed as the sum of the products of the traces and the time of flight of Γ_{x_0} in each region of linearity, see [28].

Let τ_L and τ_R be the time of flight of Γ_{x_0} along the regions σ_L and σ_R, respectively, and let $\tau_C^S(k, \varepsilon; m)$ be the time of flight from $\mathbf{q}_1^R$ to $\mathbf{q}_0^L$ obtained in Theorem 4.2. From Lemmas A.1 and A.2, when $x_0 \in [-1, x_s)$ it follows that Γ_{x_0} intersect the switching lines $\{x = -\sqrt{\varepsilon}\}$ and $\{x = \sqrt{\varepsilon}\}$ exponentially close to $\mathbf{q}_0^L$ and $\mathbf{q}_1^R$, respectively. Therefore, the values of τ_L and τ_R can be approximated by the time of flight of the orbit from $\mathbf{q}_0^L$ to $(-\sqrt{\varepsilon}, h)$ and from $(\sqrt{\varepsilon}, h)$ to $\mathbf{q}_1^R$, respectively. Hence, $\tau_L = \tau_L(h)$ and $\tau_R = \tau_R(h)$ are the ones computed in Lemma A.3. Notice that when $x_s < x_0 < -\sqrt{\varepsilon}$, we cannot assure that Γ_{x_0} intersects neither $\{x = -\sqrt{\varepsilon}\}$ nor $\{x = \sqrt{\varepsilon}\}$ exponentially close to $\mathbf{q}_0^L$ and $\mathbf{q}_1^R$, respectively, see Fig. 5. In a such case, expressions in Lemma A.3 are not good approximations to τ_L and τ_R, respectively. Therefore we have eliminated the interval $(x_s, -\sqrt{\varepsilon})$ from the scope of Theorems 4.4 and 4.6.

Then, we examine the derivative of the Poincaré map $\Pi(y_0, \boldsymbol{\kappa})$, with respect to y_0, where $y_0 = \Pi_{Cd}^{-1}(\Pi_L^{-1}(h, \boldsymbol{\kappa}), \boldsymbol{\kappa})$ and $h = \Phi_{3z}(x_0)$. This derivative corresponds to the exponential of the integral of the divergence along the limit cycle, as discussed in [27]. In the

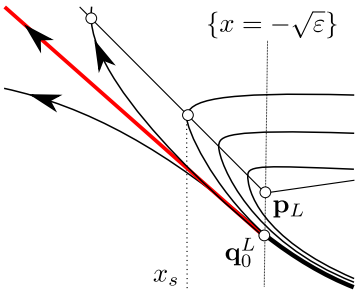

Fig. 5. Zoom of the flow in a neighborhood of the contact point $\mathbf{p}_L$. Orbits having width in $x_s < x < -\sqrt{\varepsilon}$ do not pass exponentially close of $\mathbf{q}_0^L$. Therefore, the time of flight τ_L cannot be computed as it is done in Lemma A.3.

case of PWL systems, the integral of the divergence can be explicitly computed by summing the product of the trace and the time of flight for the limit cycle in each linear region, see [28],

$$\frac{\partial \Pi}{\partial y}(y_0, \bar{\boldsymbol{\kappa}}) = e^{t_L \tau_L - m\tau_C + t_R \tau_R} + O(\varepsilon^{\frac{3}{2}}), \tag{27}$$

where $\tau_C = \tau_C^S(k, \varepsilon; m)$ and τ_{C_u} is taken into account in the term $O(\varepsilon^{\frac{3}{2}})$.

A necessary condition on the limit cycle Γ_{x_0} to be non-hyperbolic is that $\frac{\partial \Pi}{\partial y}(y_0, \bar{\boldsymbol{\kappa}}) = 1$ with $y_0 = \Pi_{Cd}^{-1}(\Pi_L^{-1}(\Phi_{3z}(x_0), \boldsymbol{\kappa}), \boldsymbol{\kappa})$. In terms of the right side of (27) this condition can be approximated by $R_{3z}(h, k, \sqrt{\varepsilon}; m) = e^{t_L \tau_L + t_R \tau_R} - e^{m\tau_C} = 0$. By using the expression of τ_L, τ_R and τ_C computed at Lemma A.3 it follows that

$$R_{3z}(h, k, \sqrt{\varepsilon}; m) = \left(1 + \frac{h + (m + \lambda_L^s)(\sqrt{\varepsilon} + a)}{(\lambda_L^q - \lambda_L^s)(\sqrt{\varepsilon} + a)}\right)^{\frac{k}{\lambda_L^s}} \left(1 + \frac{(m + \lambda_R^s)(\sqrt{\varepsilon} - a) - h}{(\lambda_R^q - \lambda_R^s)(\sqrt{\varepsilon} - a)}\right)^{\frac{1}{\lambda_R^s}} - e^{m\tau_C}. \tag{28}$$

Notice that the function R_{3z} writes in terms of the height h of the cycle Γ_{x_0}, with $h = \Phi_{3z}(x_0)$. In the next result we compute the stability of a canard cycle through the sign of the function R_{3z}.

Proposition 5.2. *For ε fixed and small enough, there exists $0 < \delta \ll 1$ such that for $x_0 \in [-1, x_s)$ and $h = \Phi_{3z}(x_0)$:*

(a) If $R_{3z}(h, k, \sqrt{\varepsilon}; m) < -\delta$, then Γ_{x_0} is a hyperbolic headless stable canard cycle.
(b) If h is a simple root of $R_{3z}(h, k, \sqrt{\varepsilon}; m)$, then in a neighborhood of Γ_{x_0} there is a nonhyperbolic headless canard cycle.
(c) If $R_{3z}(h, k, \sqrt{\varepsilon}; m) > \delta$, then Γ_{x_0} is a hyperbolic headless unstable canard cycle.

Proof. The proposition is a straightforward consequence of the definition of $R_{3z}(h, k, \varepsilon; m)$ and Eq. (27). □

By fixing parameters k and ε we next describe the qualitative behavior of $R_{3z}(h, k, \sqrt{\varepsilon}; m)$ as a function of h, both in the supercritical case, $m = -\sqrt{\varepsilon}$, and in the subcritical case, $m = \sqrt{\varepsilon}$. Even when the domain of definition of R_{3z}, as a function of h, is greater, we only consider the reduction of R_{3z} to the interval $(h_s, h_M]$ where $h_s = \Phi_{3z}(x_s)$ and $h_M = \Phi_{3z}(-1)$, see Lemma A.1. We pay special attention to the existence of simple zeros of R_{3z}.

Proposition 5.3. *Consider the function $R_{3z}(h, k, \varepsilon; m)$ defined in (28).*

(a) Under the supercritical condition $m = -\sqrt{\varepsilon}$ we obtain that:

(a-1) For $k \le 1$, then $R_{3z}(h, k, \sqrt{\varepsilon}; m) < 0$ when $h \in (h_s, h_M]$.
(a-2) For $k > 1$ and ε small enough, the function $R_{3z}(h, k, \sqrt{\varepsilon}; m)$ behaves as it is represented in Fig. 6(a). More specifically:

(a-2-1) $\lim_{h \searrow h_s} R_{3z}(h, k, \sqrt{\varepsilon}; m) < 0$ and $R_{3z}(h_M, k, \sqrt{\varepsilon}; m) > 0$,
(a-2-2) let $h^* \in (h_s, h_M]$ be a zero of $R_{3z}(h, k, \sqrt{\varepsilon}; m)$, then $\left.\frac{\partial R_{3z}}{\partial h}\right|_{(h^*, k, \sqrt{\varepsilon}; m)} > 0$, and
(a-2-3) denoting by $h^*(k, \varepsilon; m)$ the unique positive zero of $R_{3z}(h, k, \sqrt{\varepsilon}; m)$ in $(h_s, h_M]$, then

$$h^*(k, \varepsilon; m) = \frac{2}{1 + e^{\frac{\pi}{\sqrt{3}}}} k^{\frac{k^2}{k^2-1}} e^{\frac{\pi}{\sqrt{3}} \frac{k^2-2\varepsilon}{k^2-1}} \sqrt{\varepsilon} + O(\varepsilon).$$

(b) Under the subcritical condition $m = \sqrt{\varepsilon}$ we obtain that:

(b-1) For $k < 1$ and ε small enough, the function $R_{3z}(h, k, \sqrt{\varepsilon}; m)$ behaves as it is represented in Fig. 6(c). More specifically:

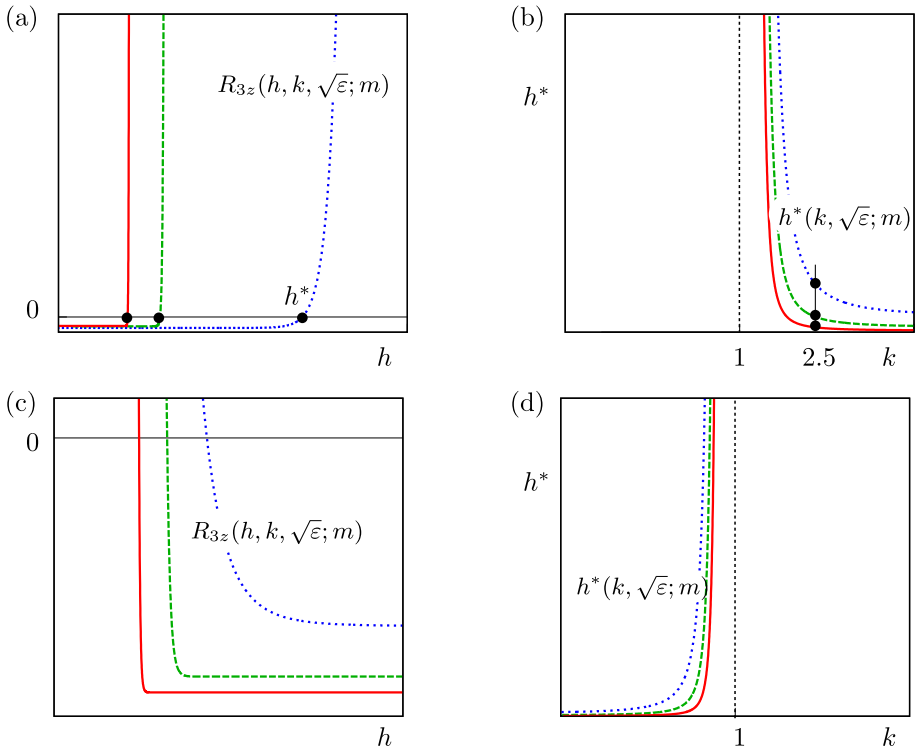

Fig. 6. Graphs of the functions $R_{3z}(h,k,\sqrt{\varepsilon};m)$ and $h^*(k,\varepsilon;m)$ in Proposition 5.3 for different values of ε. In particular, blue/dotted curves correspond with $\varepsilon = 0.05$, green/dashed curves with $\varepsilon = 0.01$ and red/solid curves with $\varepsilon = 0.005$. First column contains the graphs of the function $R_{3z}(h,k,\sqrt{\varepsilon};m)$ as a function of h for the previous values of ε: panel (a) when $k = 2.5$ and $m = -\sqrt{\varepsilon}$ and panel (c) when $k = 0.75$ and $m = \sqrt{\varepsilon}$. Second column contains the graphs of the function $h^*(k,\varepsilon;m)$ as a function of k for the previous values of ε: panel (b) when $m = -\sqrt{\varepsilon}$ and panel (d) when $m = \sqrt{\varepsilon}$.

(b-1-1) $\lim_{h\searrow h_s} R_{3z}(h,k,\sqrt{\varepsilon};m) > 0$ *and* $R_{3z}(h_M,k,\sqrt{\varepsilon};m) = -e^{\frac{2\pi}{\sqrt{3}}}$,

(b-1-2) let $h^* > 0$ *be a zero of* $R_{3z}(h,k,\sqrt{\varepsilon};m) = 0$, *then* $\frac{\partial R_{3z}}{\partial h}\Big|_{(h^*,k,\sqrt{\varepsilon}:m)} < 0$.

(b-1-3) denoting by $h^*(k,\varepsilon;m)$ *the unique zero of* $R_{3z}(h,k,\sqrt{\varepsilon};m) = 0$ *in* $(h_s,h_M]$, *then*

$$h^*(k,\varepsilon;m) = \frac{2}{1+e^{\frac{\pi}{\sqrt{3}}}} k^{\frac{k^2}{k^2-1}} e^{\frac{\pi}{\sqrt{3}}\frac{1-2\varepsilon}{1-k^2}} \sqrt{\varepsilon} + O(\varepsilon),$$

(b-2) for $k \geq 1$, *then* $R_{3z}(h,k,\sqrt{\varepsilon};m) > 0$ *when* $h \in (h_s,h_M]$.

Proof. By straightforward computations we write

$$\begin{aligned} R_{3z}(0,k,\sqrt{\varepsilon};m) &= \left(1+\frac{m+\lambda_L^s}{\lambda_L^q-\lambda_L^s}\right)^{\frac{k}{\lambda_L^s}} \left(1+\frac{m+\lambda_R^s}{\lambda_R^q-\lambda_R^s}\right)^{\frac{1}{\lambda_R^s}} - e^{m\tau_C} \\ &= \left(1+\frac{1}{\frac{\lambda_L^q-\lambda_L^s}{m+\lambda_L^s}}\right)^{\frac{k}{\lambda_L^s}} \left(1+\frac{1}{\frac{\lambda_R^q+m}{-(\lambda_R^s+m)}}\right)^{-\frac{1}{\lambda_R^s}} - e^{m\tau_C} \\ &= \left(1+\frac{1}{z_1}\right)^{\frac{k}{\lambda_L^s}} \left(1+\frac{1}{z_2}\right)^{-\frac{1}{\lambda_R^s}} - e^{m\tau_C}, \end{aligned}$$

where

$$z_1 = \frac{\lambda_L^q-\lambda_L^s}{m+\lambda_L^s} = \frac{k}{m} - 1 + O(m),$$

$$z_2 = \frac{\lambda_R^q+m}{-(m+\lambda_R^s)} = \frac{1}{m} - O(m).$$

Since z_1 and z_2 tend to ∞ or $-\infty$ depending on $s = \text{sign}(m)$, as ε tends to zero, we obtain

$$\lim_{\varepsilon \searrow 0} R_{3z}(0, k, \sqrt{\varepsilon}; m) = e^{\lim_{\varepsilon\searrow 0} \frac{1}{z_1}\frac{k}{\lambda_L^s} - \frac{1}{z_2}\frac{1}{\lambda_R^s}} - e^{s\frac{2\pi}{\sqrt{3}}} = e^{\lim_{\varepsilon\searrow 0} s\frac{k+1}{\sqrt{\varepsilon}} + 1 + O(\varepsilon^{1/2})} - e^{s\frac{2\pi}{\sqrt{3}}}.$$

Moreover, as h_s tends to zero when ε does, we conclude that $sR_{3z}(h_s, k, \sqrt{\varepsilon}; m) > 0$, provided ε is small enough.

Expanding the different operands in the expression (28) in power series of ε, and keeping the lower order terms, we obtain the following power series in ε of $R_{3z}(h, k, \sqrt{\varepsilon}; m)$ given by

$$\begin{aligned} R_{3z}(h, k, \sqrt{\varepsilon}; m) &= \left(\frac{\left(\frac{A}{\sqrt{\varepsilon}} + 1 + O(\varepsilon^{\frac{1}{2}})\right)^{k^2}}{\frac{B}{\sqrt{\varepsilon}} + 1 + O(\varepsilon^{\frac{1}{2}})} \right)^{\frac{1}{\varepsilon}} - e^{s\frac{2\pi}{\sqrt{3}}} + O(\varepsilon^{\frac{1}{2}}) \\ &= \left(\frac{A^{k^2}}{B}\right)^{\frac{1}{\varepsilon}} \varepsilon^{\frac{1-k^2}{2\varepsilon}} - e^{s\frac{2\pi}{\sqrt{3}}} + O(\varepsilon^{\frac{1-k^2}{2\varepsilon}+\frac{1}{2}}, \varepsilon^{\frac{1}{2}}), \end{aligned}$$

where A, B, and $\frac{A^{k^2}}{B}$ depends on s in the following way. If $s = 1$ then

$$A = \frac{(e^{\frac{\pi}{\sqrt{3}}} + 1)h}{2k}, \quad B = \frac{(e^{\frac{\pi}{\sqrt{3}}} + 1)h}{2e^{\frac{\pi}{\sqrt{3}}}}, \quad \frac{A^{k^2}}{B} = \frac{e^{\frac{\pi}{\sqrt{3}}}}{k}\left(\frac{(e^{\frac{\pi}{\sqrt{3}}} + 1)h}{2k}\right)^{k^2-1}$$

and, if $s = -1$ then

$$A = \frac{(e^{\frac{\pi}{\sqrt{3}}} + 1)h}{2ke^{\frac{\pi}{\sqrt{3}}}}, \quad B = \frac{(e^{\frac{\pi}{\sqrt{3}}} + 1)h}{2}, \quad \frac{A^{k^2}}{B} = \frac{1}{\left(ke^{\frac{\pi}{\sqrt{3}}}\right)^{k^2}}\left(\frac{(e^{\frac{\pi}{\sqrt{3}}} + 1)h}{2}\right)^{k^2-1}.$$

From here, we obtain the sign of the function R_{3z} at $h_M = \Phi_{3z}(-1) = k + O(\sqrt{\varepsilon})$, depending on the parameters. That is, for fixed $k > 1$ then $R_{3z}(h_M, k, \sqrt{\varepsilon}; m) > 0$ provided that ε is small enough; when $k = 1$ the sign of the function $R_{3z}(h_M, k, \sqrt{\varepsilon}; m)$ is equal to the sign of m; and for $k < 1$ then $R_{3z}(h_M, k, \sqrt{\varepsilon}; m) = -e^{s\frac{2\pi}{\sqrt{3}}} < 0$.

From the previous assertions, we conclude the existence of a zero $h^* \in (h_s, h_M]$ of the function $R_{3z}(h, k, \sqrt{\varepsilon}; m)$ for the parameters $m = -\sqrt{\varepsilon}$ and $k > 1$, and for $m = \sqrt{\varepsilon}$ and $k < 1$. The expression of h^* stated in the theorem follows by equalizing to zero the approximation of $R_{3z}(h, k, \sqrt{\varepsilon}; m)$ given above.

The partial derivative of $R_{3z}(h, k, \sqrt{\varepsilon}; m)$ with respect to h can be written as follows

$$\begin{aligned} \left.\frac{\partial R_{3z}}{\partial h}\right|_{(h,k,\sqrt{\varepsilon};m)} &= \left(R_{3z}(h, k, \sqrt{\varepsilon}; m) + e^{s\frac{2\pi}{\sqrt{3}}}\right) \\ &\quad \left(\frac{k}{\lambda_L^s((\lambda_L^q + m)(\sqrt{\varepsilon} + a) + h)} - \frac{1}{\lambda_R^s((\lambda_R^q + m)(\sqrt{\varepsilon} - a) - h)}\right) \\ &= \left(R_{3z}(h, k, \sqrt{\varepsilon}; m) + e^{s\frac{2\pi}{\sqrt{3}}}\right)\left(\frac{k^2 - 1}{hm^2} + O(\varepsilon^{-\frac{1}{2}})\right). \end{aligned}$$

Therefore, assuming the existence of a zero h^* of $R_{3z}(h, k, \sqrt{\varepsilon}; m)$, we obtain that $\left.\frac{\partial R_{3z}}{\partial h}\right|_{(h^*,k,\sqrt{\varepsilon})} < 0$ if $k < 1$, and $\left.\frac{\partial R_{3z}}{\partial h}\right|_{(h^*,k,\sqrt{\varepsilon})} > 0$ if $k > 1$, which implies the uniqueness of such zero. From here, we conclude that function R_{3z} does not change sign in $(h_s, h_M]$ neither when $m = -\sqrt{\varepsilon}$ and $k \leq 1$ nor when $m = \sqrt{\varepsilon}$ and $k \geq 1$. □

5.3.2. Hyperbolicity/non-hyperbolicity of canard cycles with head

As in the previous section, we start this one by defining the Poincaré map in neighborhood of orbits visiting the four regions σ_{LL}, σ_L, σ_C and σ_R. Consider the Poincaré half-maps Π_{Cd}, Π_{Cu}, Π_R, and the time of flight τ_{Cd}, τ_{Cu}, and τ_R previously defined.

Let $\mathbf{p}_1 = (-\sqrt{\varepsilon}, y_1)$ be a point in the switching line $\{x = -\sqrt{\varepsilon}\}$ and located below the point $\mathbf{p}_L$, and assume that there exists a time of flight $\tau_{Ld} > 0$ such that $x^L(\tau_{Ld}; \mathbf{p}_1, \boldsymbol{\kappa}) = -1$ and $-1 < x^L(t; \mathbf{p}_1, \boldsymbol{\kappa}) < -\sqrt{\varepsilon}$ for all $t \in (0, \tau_{Ld})$. In such a case, we define the Poincaré half-map between the switching lines $\{x = -\sqrt{\varepsilon}\}$ and $\{x = -1\}$ at the point y_1 as $\Pi_{Ld}(y_1, \boldsymbol{\kappa}) = y^L\left(\tau_{Ld}; \mathbf{p}_1, \boldsymbol{\kappa}\right)$. Moreover, consider a point $\mathbf{p}_2 = (-1, y_2)$ located below the point $\mathbf{p}_{LL}$ and assume that there exists a time of flight $\tau_{LL} > 0$ such that $x^{LL}(\tau_{LL}; \mathbf{p}_1, \boldsymbol{\kappa}) = -1$ and $x^{LL}(t; \mathbf{p}_1, \boldsymbol{\kappa}) < -1$ for all $t \in (0, \tau_{LL})$. We define the Poincaré half-map between the switching line $\{x = -1\}$ and itself at the point y_2 as $\Pi_{LL}(y_2, \boldsymbol{\kappa}) = y^{LL}\left(\tau_{LL}; \mathbf{p}_2, \boldsymbol{\kappa}\right)$. Finally, let $\mathbf{p}_3 = (-1, y_3)$ be a point in the switching line $\{x = -1\}$, located over the point $\mathbf{p}_{LL}$, and assume that there exists $\tau_{Lu} > 0$ such that $x^L(\tau_{Lu}; \mathbf{p}_3, \boldsymbol{\kappa}) = -\sqrt{\varepsilon}$ and $-1 < x^L(t; \mathbf{p}_3, \boldsymbol{\kappa}) < -\sqrt{\varepsilon}$ for all $t \in (0, \tau_{Lu})$. We define the Poincaré half-map between the switching lines $\{x = -1\}$ and $\{x = -\sqrt{\varepsilon}\}$ at the point y_3 as $\Pi_{Lu}(y_3, \boldsymbol{\kappa}) = y^L\left(\tau_{Lu}; \mathbf{p}_3, \boldsymbol{\kappa}\right)$.

At this point, the Poincaré map for an orbit of system (4) visiting zones σ_{LL}, σ_L, σ_C and σ_R can be defined.

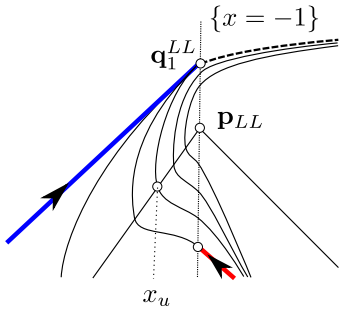

Fig. 7. Zoom of the flow in a neighborhood of the contact point $\mathbf{p}_{LL}$. Orbits having width in $x_u < x_0 < -1$ do not pass exponentially close of $\mathbf{q}_1^{LL}$. Therefore, the time of flight τ_{LL} cannot be computed as in Lemma A.3.

Definition 5.4. The Poincaré map Π in the neighborhood of an orbit Γ_{x_0} of system (4) visiting zones σ_{LL}, σ_L, σ_C and σ_R is defined as

$$\Pi(y_0,\boldsymbol{\kappa}) = \Pi_R(\Pi_{Cu}(\Pi_{Lu}(\Pi_{LL}(\Pi_{Ld}(\Pi_{Cd}(y_0,\boldsymbol{\kappa}),\boldsymbol{\kappa}),\boldsymbol{\kappa}),\boldsymbol{\kappa}),\boldsymbol{\kappa}),\boldsymbol{\kappa}),$$

provided the composition of Poincaré half-maps is possible, where $y_0 = \Pi_{Cd}^{-1}(\Pi_{Ld}^{-1}(\boldsymbol{\Phi}_{4z}(x_0),\boldsymbol{\kappa}),\boldsymbol{\kappa})$.

For ε fixed and small enough, suppose the existence of a canard limit cycle with head Γ_{x_0}, see Fig. 2, obtained under the parameter relation $a = a_N(k,\varepsilon,x_0;m)$ given in Theorem 4.3. The cycle Γ_{x_0} corresponds to the fixed point of the Poincaré map $\Pi(y_0,\boldsymbol{\kappa})$, where $y_0 = \Pi_{Cd}^{-1}(\Pi_{Ld}^{-1}(\boldsymbol{\Phi}_{4z}(x_0),\boldsymbol{\kappa}),\boldsymbol{\kappa})$.

The non-hyperbolicity of Γ_{x_0} can be obtained, similarly as in the case of headless canard cycles, through the sum of the products of the traces of the matrices of the differential linear systems, and the corresponding time of flight, namely $\tau_{Cd}, \tau_{Ld}, \tau_{LL}, \tau_{Lu}, \tau_{Cu}$, and τ_R.

By analogous arguments than those for headless canard limit cycles, we conclude that $\tau_{Cd} = \tau_C^S(k,\varepsilon;m)$ obtained in Theorem 4.2, and that the values of τ_{Cu} and τ_{Lu} are negligible. On the other hand, when $x_0 \in (x_r, x_u)$ the canard cycle Γ_{x_0} intersects the switching line $\{x=-1\}$ exponentially close to $\mathbf{q}_1^{LL}$, see Lemmas A.1 and A.2. Therefore, the value of τ_{LL} can be approximated by the time of flight of Γ_{x_0} from the point $(-1,h)$, where $h = \boldsymbol{\Phi}_{4z}(x_0)$, to the point $\mathbf{q}_1^{LL}$. Then, from Lemma A.3, we obtain $\tau_{LL} = \tau_{LL}(h)$ and

$$\tau_R = \tau_R(h_0) = -\frac{1}{\lambda_R^s}\ln\left(1 + \frac{\lambda_R^s(\sqrt{\varepsilon}-a) + \lambda_{LL}^s(1+a) + k(\sqrt{\varepsilon}-1) + 2m\sqrt{\varepsilon}}{(\lambda_R^q - \lambda_R^s)(\sqrt{\varepsilon}-a)}\right), \tag{29}$$

where $h_0 = -\lambda_{LL}^s(1+a) - k(\sqrt{\varepsilon}-1) - m(\sqrt{\varepsilon}+a)$ is the second coordinate of $\mathbf{q}_1^{LL}$. Notice that when $x_u < x_0 < -1$, we cannot assure that Γ_{x_0} intersects $\{x=-1\}$ exponentially close to $\mathbf{q}_1^{LL}$, see Fig. 7. In this case, neither expression in Lemma A.3 nor expression (29) are good approximations for τ_{LL} and τ_R, respectively. Therefore, we have eliminated the interval $(x_u,-1)$ from the stated of Theorems 4.4 and 4.6.

Following similar arguments that those applied in Section 5.3, a necessary condition on the canard cycle Γ_{x_0} to be non-hyperbolic can be approximated by $R_{4z}(h,k,\varepsilon;m) = e^{t_L\tau_{Ld}+t_{LL}\tau_{LL}+t_R\tau_R} - e^{m\tau_C} = 0$. By using the expressions of $\tau_{Ld}, \tau_{LL}, \tau_R$ and τ_C in Lemma A.3 we obtain

$$\begin{aligned} R_{4z}(h,k,\sqrt{\varepsilon};m) = &\left(1 + \frac{h + m(\sqrt{\varepsilon}+a) + \lambda_L^s(2\sqrt{\varepsilon}+a-1)}{(\lambda_L^q - \lambda_L^s)(\sqrt{\varepsilon}+a)}\right)^{\frac{k}{\lambda_L^s}} \\ &\left(1 + \frac{h + m(\sqrt{\varepsilon}+a) + k(\sqrt{\varepsilon}-1) + \lambda_{LL}^s(1+a)}{(\lambda_{LL}^q - \lambda_{LL}^s)(1+a)}\right)^{\frac{1}{\lambda_{LL}^s}} \\ &\left(1 + \frac{\lambda_R^s(\sqrt{\varepsilon}-a) + \lambda_{LL}^s(1+a) + k(\sqrt{\varepsilon}-1) + 2m\sqrt{\varepsilon}}{(\lambda_R^q - \lambda_R^s)(\sqrt{\varepsilon}-a)}\right)^{\frac{1}{\lambda_R^s}} - e^{m\tau_C}. \end{aligned} \tag{30}$$

In the next result, we find the stability of a canard cycle with head, through the sign of function R_{4z}

Proposition 5.5. *For ε fixed and small enough, there exists $0 < \delta \ll 1$, such that, for $x_0 \in (x_r, x_u)$ and $h = \boldsymbol{\Phi}_{4z}(x_0)$:*

(a) If $R_{4z}(h,k,\sqrt{\varepsilon};m) < -\delta$, then Γ_{x_0} is a hyperbolic stable canard cycle with head.
(b) If h is a simple root of $R_{4z}(h,k,\sqrt{\varepsilon};m)$, then in a neighborhood of Γ_{x_0} there is a nonhyperbolic canard cycle with head.
(c) If $R_{4z}(h,k,\sqrt{\varepsilon};m) > \delta$, then Γ_{x_0} is a hyperbolic unstable canard cycle with head.

Proof. The proposition follows similarly to Proposition 5.2. □

Next, we describe the qualitative behavior of $R_{4z}(h,k,\sqrt{\varepsilon};m)$, as a function of h, for fixed values of the parameters k and ε. Even when the domain of the function R_{4z} is greater, we consider it reduced to (h_r,h_u), where $h_r=\Phi_{4z}(x_r)$ and $h_u=\Phi_{4z}(x_u)$, see Lemma A.1.

Proposition 5.6. *Consider the function $R_{4z}(h,k,\varepsilon;m)$ defined in (30).*

(a) If $k<1$, or $k=1$ and $m=-\sqrt{\varepsilon}$, and ε small enough, then $R_{4z}(h,k,\sqrt{\varepsilon};m)<0$ in (h_r,h_u).

(b) If $k>1$, or $k=1$ and $m=\sqrt{\varepsilon}$, and ε small enough, then $R_{4z}(h,k,\sqrt{\varepsilon};m)$ behaves as in Fig. 8(a) or in Fig. 8(c), depending on the supercritical case, $m=-\sqrt{\varepsilon}$, or the subcritical case, $m=\sqrt{\varepsilon}$, respectively. More specifically:

(b-1) $R_{4z}(h_r,k,\sqrt{\varepsilon};m)<0$ and $R_{4z}(h_u,k,\sqrt{\varepsilon};m)>0$, see Fig. 8(a) and (c);

(b-2) let $h^*\in(h_r,h_u)$ be a zero of $R_{4z}(h,k,\sqrt{\varepsilon};m)$, then $\left.\frac{\partial R_{4z}}{\partial h}\right|_{(h^*,k,\sqrt{\varepsilon};m)}>0$;

(b-3) denoting by $h^*(k,\sqrt{\varepsilon};m)$ the unique zero of $R_{4z}(h,k,\varepsilon;m)$ in (h_r,h_u), it follows that, if $k>1$, then

$$h^*(k,\sqrt{\varepsilon};m)=(k+1)e^{\frac{2-k^2}{2}}(\sqrt{\varepsilon})^{\frac{k^2-1}{k^2}}+O(\sqrt{\varepsilon}),$$

see Fig. 8(b) and (d), and if $k=1$ then

$$h^*(1,\sqrt{\varepsilon};m)=\frac{2}{1+e^{\frac{\pi}{\sqrt{3}}}}+O(\sqrt{\varepsilon}),$$

see Fig. 8(d).

Proof. Setting $m=\pm\sqrt{\varepsilon}$ and $s=\operatorname{sign}(m)$, and expanding in power series of ε every term in the expression of $R_{4z}(h,k,\sqrt{\varepsilon};m)$, we obtain that

$$\begin{aligned}R_{4z}(h,k,\sqrt{\varepsilon};m)=&\left(1+k-h-\frac{2k+h(e^{s\frac{\pi}{\sqrt{3}}}-1)}{1+e^{s\frac{\pi}{\sqrt{3}}}}\sqrt{\varepsilon}+O(\varepsilon)\right)^{-\frac{1}{\varepsilon}+1+O(\varepsilon)}\\&\left(\frac{k(1+e^{-s\frac{\pi}{\sqrt{3}}})}{2}\frac{1}{\sqrt{\varepsilon}}-\frac{k(1+e^{-s\frac{\pi}{\sqrt{3}}})-2}{2}+O(\varepsilon^{\frac{1}{2}})\right)^{-\frac{1}{\varepsilon}+1+O(\varepsilon)}\\&\left(\frac{h(1+e^{s\frac{\pi}{\sqrt{3}}})}{2k}\frac{1}{\sqrt{\varepsilon}}+1-\left(\frac{e^{s\frac{\pi}{\sqrt{3}}}+1-2ks}{2k^2}+\frac{e^{s\frac{\pi}{\sqrt{3}}}(k^2-5)-4}{4k^3}h\right)\sqrt{\varepsilon}+O(\varepsilon)\right)^{\frac{k^2}{\varepsilon}-1+O(\varepsilon)}\\&-e^{s\frac{2\pi}{\sqrt{3}}-s\frac{k+1}{k}\sqrt{\varepsilon}+O(\varepsilon)}.\end{aligned}$$

By changing the sign in the exponent of the first two terms, it follows that

$$\begin{aligned}R_{4z}(h,k,\sqrt{\varepsilon};m)=&\left(\frac{1}{1+k-h}+\frac{2k+h(e^{s\frac{\pi}{\sqrt{3}}}-1)}{\left(1+e^{s\frac{\pi}{\sqrt{3}}}\right)(1+k-h)^2}\sqrt{\varepsilon}+O(\varepsilon)\right)^{\frac{1}{\varepsilon}-1+O(\varepsilon)}\\&\left(\frac{2}{k(1+e^{-s\frac{\pi}{\sqrt{3}}})}\sqrt{\varepsilon}+O(\varepsilon)\right)^{\frac{1}{\varepsilon}-1+O(\varepsilon)}\\&\left(\frac{h(1+e^{s\frac{\pi}{\sqrt{3}}})}{2k}\frac{1}{\sqrt{\varepsilon}}+1-\left(\frac{e^{s\frac{\pi}{\sqrt{3}}}+1-2ks}{2k^2}+\frac{e^{s\frac{\pi}{\sqrt{3}}}(k^2-5)-4}{4k^3}h\right)\sqrt{\varepsilon}+O(\varepsilon)\right)^{\frac{k^2}{\varepsilon}-1+O(\varepsilon)}\\&-e^{s\frac{2\pi}{\sqrt{3}}-s\frac{k+1}{k}\sqrt{\varepsilon}+O(\varepsilon)}.\end{aligned}\tag{31}$$

Then

$$\begin{aligned}R_{4z}(0,k,\sqrt{\varepsilon};m)=&\left(\frac{1}{1+k}+O(\sqrt{\varepsilon})\right)^{\frac{1}{\varepsilon}-1+O(\varepsilon)}\left(\frac{2}{k(1+e^{-s\frac{\pi}{\sqrt{3}}})}\sqrt{\varepsilon}+O(\varepsilon)\right)^{\frac{1}{\varepsilon}-1+O(\varepsilon)}\\&\left(1-\frac{e^{s\frac{\pi}{\sqrt{3}}}+1-2sk}{2k^2}\sqrt{\varepsilon}+O(\varepsilon)\right)^{\frac{k^2}{\varepsilon}-1+O(\varepsilon)}\end{aligned}$$

$$- e^{s\frac{2\pi}{\sqrt{3}}} + O(\sqrt{\varepsilon}),$$

which can be expanded in power series of ε as follows

$$R_{4z}(0,k,\sqrt{\varepsilon};m) = \left(\frac{2\sqrt{\varepsilon}}{k(1+k)(1+e^{-s\frac{\pi}{\sqrt{3}}})} - \frac{(e^{s\frac{\pi}{\sqrt{3}}}+1-2sk)\varepsilon}{k(1+k)(1+e^{-s\frac{\pi}{\sqrt{3}}})} + O(\varepsilon^{\frac{3}{2}})\right)^{\frac{1}{\varepsilon}} - e^{s\frac{2\pi}{\sqrt{3}}} + O(\sqrt{\varepsilon}).$$

The first operand in the right side of previous equation tends to zero provided that ε does. Hence, for ε small enough we obtain that $-e^{s\frac{2\pi}{\sqrt{3}}} < R_{4z}(0,k,\sqrt{\varepsilon};m) < 0$. Same expression is also satisfied by $R_{4z}(h_r,k,\sqrt{\varepsilon};m)$ since $\lim_{\varepsilon\searrow 0} h_r = 0$. Thus, we conclude that $-e^{s\frac{2\pi}{\sqrt{3}}} < R_{4z}(h_r,k,\sqrt{\varepsilon};m) < 0$.

On the other hand, from expression (31) it follows that

$$\begin{aligned} R_{4z}(k,k,\sqrt{\varepsilon};m) &= \left(1+k\sqrt{\varepsilon}+O(\varepsilon)\right)^{\frac{1}{\varepsilon}-1+O(\varepsilon)} \left(\frac{2}{k(1+e^{-s\frac{\pi}{\sqrt{3}}})}\sqrt{\varepsilon}+O(\varepsilon)\right)^{\frac{1}{\varepsilon}-1+O(\varepsilon)} \\ &\quad \left(\frac{1+e^{s\frac{\pi}{\sqrt{3}}}}{2}\frac{1}{\sqrt{\varepsilon}}+1+O(\sqrt{\varepsilon})\right)^{\frac{k^2}{\varepsilon}-1+O(\varepsilon)} - e^{s\frac{2\pi}{\sqrt{3}}-s\frac{k+1}{k}\sqrt{\varepsilon}+O(\varepsilon)} \\ &= \left(\frac{2^{1-k^2}(1+e^{s\frac{\pi}{\sqrt{3}}})^{k^2-1}e^{s\frac{\pi}{\sqrt{3}}}}{k}\varepsilon^{\frac{1-k^2}{2}} + O\left(\varepsilon^{\frac{2-k^2}{2}}\right)\right)^{\frac{1}{\varepsilon}} - e^{s\frac{2\pi}{\sqrt{3}}}. \end{aligned}$$

Hence, for ε small enough we obtain that if $k > 1$, then $R_{4z}(k,k,\sqrt{\varepsilon};m) > 0$; and if $k < 1$, then $R_{4z}(k,k,\sqrt{\varepsilon};m) < 0$. Moreover, when $k = 1$ it follows that $R_{4z}(k,k,\sqrt{\varepsilon};m)$ has the same sign than m. Since $\lim_{\varepsilon\searrow 0} h_u = k$, previous inequalities are also satisfied by $R_{4z}(h_u,k,\sqrt{\varepsilon};m)$.

Let $h_r < h^* < h_u$ be a zero of $R_{4z}(h,k,\sqrt{\varepsilon};m)$. Straightforward computations shows that

$$\left.\frac{\partial R_{4z}}{\partial h}\right|_{(h^*,k,\sqrt{\varepsilon};m)} = e^{s\frac{2\pi}{\sqrt{3}}-s\frac{k+1}{k}\sqrt{\varepsilon}+O(\varepsilon)}\left(\frac{k^3+k^2(1-h^*)+h^*}{h^*(k+1-h^*)\varepsilon}+O\left(\frac{1}{\sqrt{\varepsilon}}\right)\right) > 0,$$

which implies that, when it exists, the zero h^* is unique. Moreover, by keeping the lower order terms in (31), we obtain the following implicit expression for an approximation to the solution $h^*(k,\sqrt{\varepsilon})$ of $R_{4z}(h,k,\sqrt{\varepsilon};m) = 0$, that is,

$$\left(\frac{1}{1+k-h^*}\right)\left(\frac{2\sqrt{\varepsilon}}{k(1+e^{-s\frac{\pi}{\sqrt{3}}})}\right)\left(\frac{h^*(1+e^{s\frac{\pi}{\sqrt{3}}})}{2k}\frac{1}{\sqrt{\varepsilon}}\right)^{k^2} = e^{s\frac{2\pi}{\sqrt{3}}\varepsilon}.$$

When $k = 1$, the equation above can be solved and it follows that

$$h^* = \frac{2}{1+e^{s\frac{\pi}{\sqrt{3}}}} + O(\sqrt{\varepsilon}),$$

which implies that $h^* < h_u$ only if $m = \sqrt{\varepsilon}$. When $k \neq 1$ the solution of the equation can be approximated by the undetermined coefficients method

$$h^* = (k+1)e^{\frac{2-k^2}{2}}(\sqrt{\varepsilon})^{\frac{k^2-1}{k^2}} + O(\sqrt{\varepsilon}). \quad \square$$

In Fig. 8(a) we represent $R_{4z}(h,k,\varepsilon;m)$ as a function of h for different values of ε and $k > 1$. We notice that function $R_{4z}(h,k,\varepsilon;m)$ is negative for h close to h_r, and positive for values close to h_u. Moreover, as it follows from the proof of the previous theorem, $\lim_{\varepsilon\searrow 0} R_{4z}(0,k,\sqrt{\varepsilon};m) = -e^{\frac{2\pi}{\sqrt{3}}}$. Furthermore, the unique zero $h^*(k,\sqrt{\varepsilon})$ tends to zero as ε tends to zero. In Fig. 8(b) we represent function $h^*(k,\sqrt{\varepsilon})$ as a function of k for different values of ε. Notice that all the curves have a common point at $k = 1$ and $h^* = 2e^{\frac{1}{2}} \approx 3.297442541400256\ldots > k$, which lies out of the interval (h_r,h_u) since $h_u \approx k$. Therefore, this part of the curves do not correspond to non-hyperbolic canard cycles, see Fig. 9.

5.3.3. Correspondence to saddle–node bifurcations

To finish with the proof of Theorems 4.4 and 4.6, in this subsection we are going to prove that the non-hyperbolic canard limit cycles whose existence has been proved in the previous sections correspond, indeed, to a saddle–node bifurcation. We start with the proof in the case of headless canard cycles.

We will prove that the non-degeneracy conditions on the Poincaré map hold, that is, the second derivative of the Poincaré map with respect to the initial condition and the derivative of the Poincaré map with respect to parameter a are both different from zero, see [34,35].

Consider a non-hyperbolic headless canard cycle Γ_{x_0} corresponding to a fixed point of the Poincaré map y_0 for parameters $\boldsymbol{\kappa} = \bar{\boldsymbol{\kappa}}$, i.e. $y_0 = \Pi_{Cd}^{-1}(\Pi_L^{-1}(\boldsymbol{\Phi}(x_0),\bar{\boldsymbol{\kappa}}),\bar{\boldsymbol{\kappa}})$. First, we compute the second derivative of the Poincaré map with respect to the initial condition

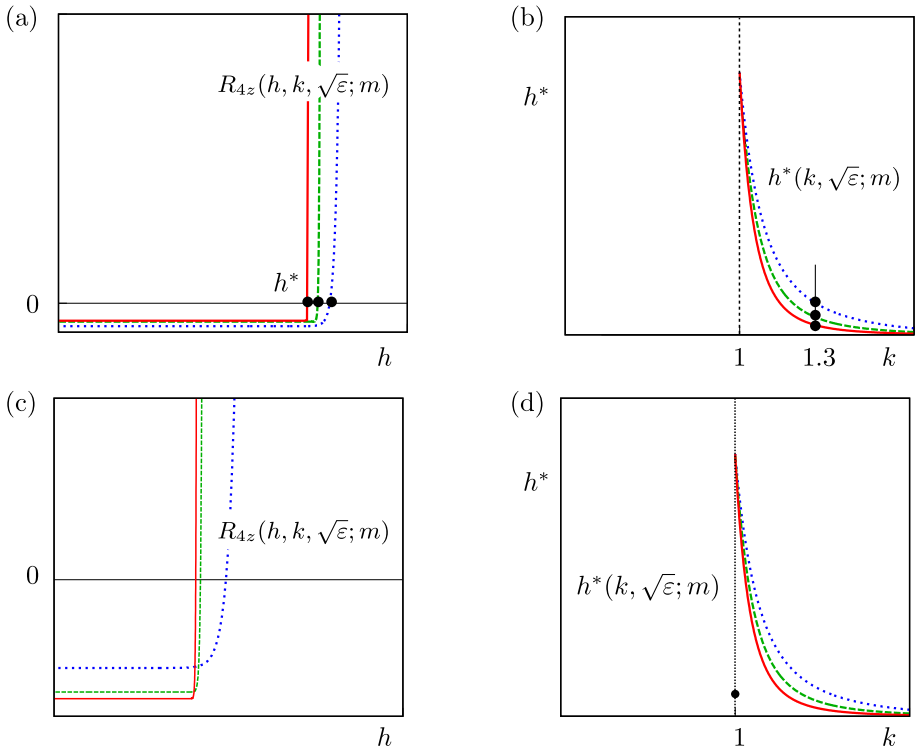

Fig. 8. Graphs of the functions $R_{4z}(h,k,\sqrt{\varepsilon};m)$ and $h^*(k,\varepsilon;m)$ in Proposition 5.6 for different values of ε. In particular blue/dotted curves correspond with $\varepsilon = 0.05$, green/dashed curves with $\varepsilon = 0.01$ and red/solid curves with $\varepsilon = 0.005$. First column contains the graphs of the function $R_{4z}(h,k,\sqrt{\varepsilon};m)$ as a function of h for the previous values of ε: panel (a) when $k = 1.3$ and $m = -\sqrt{\varepsilon}$ and panel (c) when $k = 0.75$ and $m = \sqrt{\varepsilon}$. Second column contains the graphs of the function $h^*(k,\varepsilon;m)$ as a function of k for the previous values of ε: panel (b) when $m = -\sqrt{\varepsilon}$ and panel (d) when $m = \sqrt{\varepsilon}$.

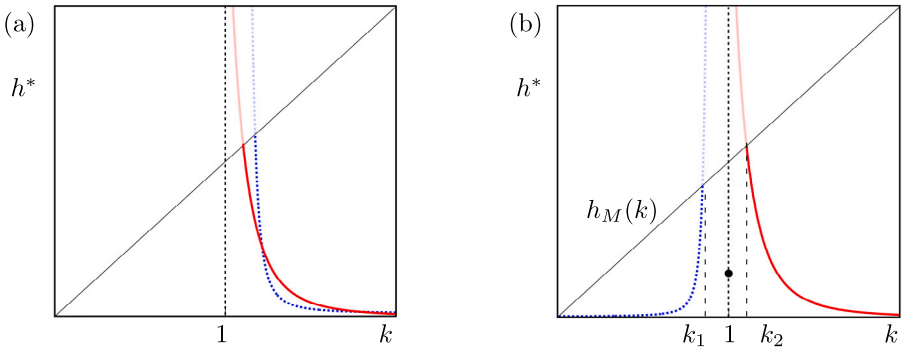

Fig. 9. Curves of saddle–node canard cycles of system (4) with $\epsilon = 1e-5$. Pointed/blue curves correspond with three zonal saddle–node canard cycles (headless canards). Solid/red curves correspond with four zonal saddle–node canard cycles (canards with head). The diagonal is the value of the height h_M as a function of k. The part of the curves over the diagonal corresponds to zeros of the function R_{3z} and R_{4z} which are not saddle–node canards. Panel (a) represents the two saddle–node canard cycles appearing in the supercritical case $m = -\sqrt{\epsilon}$ for $k > 1$. Panel (b) represents the saddle–node canard cycles appearing in the subcritical case $m = \sqrt{\epsilon}$, in this case for each value of k only one saddle–node limit cycle can appears.

and we will see that, in a headless non-hyperbolic canard cycle this derivative is nonzero if and only function R_{3z} is non zero at $\bar{h} = \Phi_{3z}(x_0)$. Second, we compute the derivative of the Poincaré map with respect to parameter a and we test that this derivative does not vanish.

From expression (27), the second derivative of Poincaré map with respect to h in the non-hyperbolic fixed point $\bar{h}$ is given by

$$\frac{\partial^2 \Pi}{\partial y^2}(y_0, \bar{\boldsymbol{\kappa}}) = \frac{\partial G}{\partial h}(\bar{h}, \bar{\boldsymbol{\kappa}}), \tag{32}$$

where

$$G(h,\boldsymbol{\kappa}) = e^{t_L\tau_L - m\tau_C + t_R\tau_R}.$$

It is easy to see that

$$G(h,\boldsymbol{\kappa}) = (R_{3z}(h,k,\sqrt{\varepsilon};m) + e^{m\tau_C})e^{-m\tau_C} = R_{3z}(h,k,\sqrt{\varepsilon};m)e^{-m\tau_C} + 1.$$

As in a non-hyperbolic headless canard cycle $R_{3z}(h,k,\sqrt{\varepsilon};m) = 0$, it is easy to see that,

$$\frac{\partial G}{\partial h}(\bar{h},\bar{\boldsymbol{\kappa}}) = \frac{\partial R_{3z}}{\partial h}(\bar{h},\bar{\boldsymbol{\kappa}})e^{-m\tau_C}.$$

Thus, from expression (32), in a non-hyperbolic headless canard cycle,

$$\frac{\partial^2 \Pi}{\partial y^2}(y_0,\bar{\boldsymbol{\kappa}}) = \frac{\partial R_{3z}}{\partial h}(\bar{h},\bar{\boldsymbol{\kappa}})e^{-m\tau_C}, \tag{33}$$

and then the sign of $\frac{\partial^2 \Pi}{\partial y^2}(y_0,\bar{\boldsymbol{\kappa}})$ is that of $\frac{\partial R_{3z}}{\partial h}(\bar{h},\bar{\boldsymbol{\kappa}})$, which is non zero from Proposition 5.3 (a-2-2), (b-1-2) and Proposition 5.6 (b-2). To compute the derivative of the Poincaré map with respect to parameter a in the neighborhood of a non-hyperbolic headless canard cycle Γ_{x_0}, we will use the following reasoning. Taking a point $(\sqrt{\varepsilon},y_1)$ in a neighborhood of $(\sqrt{\varepsilon},y_0)$ where $y_0 = \Pi_{Cd}^{-1}(\Pi_L^{-1}(\Phi_{3z}(x_0),\boldsymbol{\kappa}),\boldsymbol{\kappa})$. The image through the Poincaré map of y_1, that is $\Pi(y_1,\boldsymbol{\kappa})$, will be exponentially close to the second component of $\mathbf{q}_1^R$, that is,

$$\Pi(y_1,\boldsymbol{\kappa}) = (m+\lambda_R^s)(\sqrt{\varepsilon}-a) + \chi(y_1,\boldsymbol{\kappa}),$$

with function $\chi(y_1,\boldsymbol{\kappa})$ and its derivatives $O(\exp(-c/\varepsilon))$ small, where c is a positive constant depending on y_1. Hence,

$$\frac{\partial \Pi}{\partial a}(y_1,\boldsymbol{\kappa}) = -(m+\lambda_R^s) + \frac{\partial \chi}{\partial a}(y_1,\boldsymbol{\kappa}) \simeq -m+\varepsilon,$$

and $\frac{\partial \Pi}{\partial a}(y_1,\boldsymbol{\kappa}) \neq 0$ as $m = \pm\sqrt{\varepsilon} \neq 0$. This implies that every non-hyperbolic canard cycles obtained in the proof of Proposition 5.2 are saddle–node canard cycles.

Regarding the proof in the case of canard cycles with head (obtained in Proposition 5.5) we proceed in a similar way by using now function R_{4z} to describe the analogous of the function G in expression (32).

By combining in a suitable way the results obtained in Proposition 5.2 and in Proposition 5.5 we conclude the proof of Theorem 4.4 and of Theorem 4.6.

5.4. Proof of Theorem 4.7

In Fig. 6(a) we draw the graph of the function $R_{3z}(h,k,\sqrt{\varepsilon};m)$ as a function of h by fixing parameter $k = 2.5$ and parameter $\varepsilon \in \{0.05, 0.01, 0.005\}$. As it has been obtained in the proof of Proposition 5.3, $R_{3z}(h,k,\sqrt{\varepsilon};m)$ tends to $-e^{\frac{2\pi}{\sqrt{3}}}$ as h decrease to h_s, and it tends to ∞ as h tends to h_M. In panel (a) we also represent the zero, $h^* \in (h_s,h_M]$, at which the function changes the sign. As it can be observed, this tends to zero as ε tends to zero.

From Proposition 5.3(c), in Fig. 6(b) we draw function $h^*(k,\sqrt{\varepsilon})$ for different values of $k<1$. As it can be observed, for a fixed $k<1$, the height of the saddle–node tends to zero assuming ε does. We conclude that fixed k the singular limit of every saddle–node is the equilibrium point at the fold.

Nevertheless, for any $h_0 \in (h_s,h_M] \cup (h_r,h_u)$, we prove that there exists a suitable election of the parameter k such that

$$\lim_{\varepsilon \searrow 0} h^*(k(\varepsilon),\varepsilon;m) = h_0,$$

which means that we can chose parameter k in such a way that the singular limit of the saddle–node is a singular cycle of prefixed height, h_0.

Next, we address the supercritical case $m = -\sqrt{\varepsilon}$ and $h_0 \in (h_s,h_M]$. The remainder cases follow by similar arguments. In order to obtain the parameter value k allowing the existence of a saddle–node canard cycle with height h_0, we use implicit equation $h^*(k,\varepsilon;m) = h_0$, where the function $h^*(k,\varepsilon;m)$ is given in Proposition 5.3(a-2-3). Since the partial derivative

$$\frac{\partial h^*}{\partial k}(k,\varepsilon;m) = \frac{2\sqrt{\varepsilon}k^{\frac{k^2}{k^2-1}+1}e^{\frac{\pi\left(k^2-2\varepsilon\right)}{\sqrt{3}\left(k^2-1\right)}}\left(2\sqrt{3}\pi(2\varepsilon-1)+3k^2-6\ln(k)-3\right)}{3\left(1+e^{\frac{\pi}{\sqrt{3}}}\right)\left(k^2-1\right)^2},$$

is different from zero when k is greater but close to 1 and $\varepsilon > 0$, the Implicit Function Theorem can be applied, and there exists $k(h,\varepsilon;m)$ such that the differential system (4) with parameters $k = k(h,\varepsilon;m)$ and $a = a_N(k(h,\varepsilon;m),\varepsilon,x_0;m)$ exhibits the saddle–node canard Γ_{x_0}, with $x_0 = \Phi_{3z}^{-1}(h)$, whose existence has been stated in Theorem 4.4, finishing the proof.

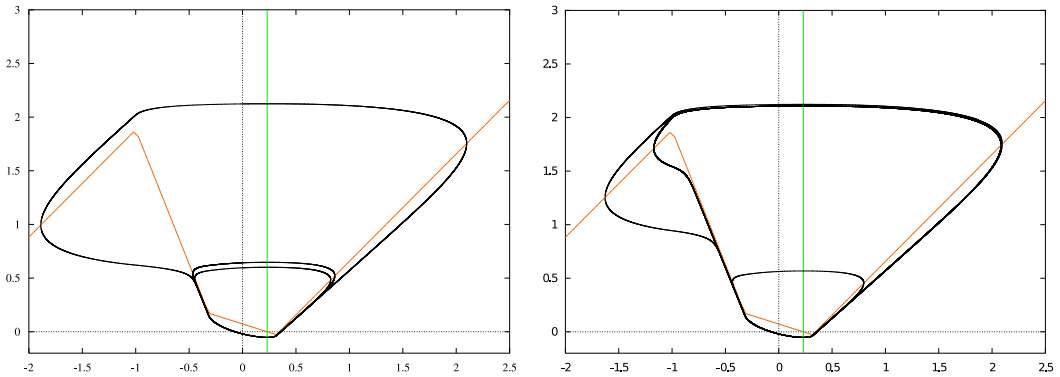

Fig. 10. Coexistence of three canard limit cycles. Simulation of three canard limit cycles close to a saddle–node configuration for the supercritical case $m = -\sqrt{\varepsilon}$. According with Fig. 9(a) two configuration are possible when $k > 1$: a saddle–node canard cycle without head and saddle–node canard cycle with head. Panel (a) depicts a configuration close to the saddle–node canard cycle without head for $\varepsilon = 0.1$, $k = 2.5$ and $a = a_1 = 0.2305968812$. The three canard cycles have initial conditions $(0, 0.595), (0, 0.642), (0, 2.12361)$. Panel (b) depicts a configuration close to the saddle–node canard cycle with head for $\varepsilon = 0.1$, $k = 2.5$ and $a = a_2 = 0.23059688315966$, the three canard cycles have initial conditions $(0, 0.561), (0, 2.10673), (0, 2.12)$. Note that $|a_1 - a_2| \approx 2e - 9 \approx e^{-\frac{2}{\varepsilon}}$, then both saddle–node canard cycles take place exponentially close.

6. Conclusions and perspectives

In this work we have analyzed the canard explosion in the PWL framework, both under supercritical and under subcritical conditions, paying special attention to the saddle–node bifurcations of canards cycles. In particular, counterparts to results in [3] have been derived in the PWL context. As we have already commented, there, the authors considered two different scenarios, depending whether the Hopf bifurcation where the family of cycles is born is supercritical or subcritical. Here, we point out the similarities and differences that we have found in this study in both cases:

- In [3], canard cycles develop along a branch born at a Hopf bifurcation, at $a = a_H$, and the canard explosion takes place at a value which is at a distance of $O(\varepsilon)$ from the a_H. In the PWL context, we have checked that the canard explosion takes place at a value a_S which is at a distance of $O(\sqrt{\varepsilon})$ from the a_H. This result is compatible with the approximation to the critical value obtained in [17]. The distance between the Hopf-like bifurcation and the canard explosion is $O(\sqrt{\varepsilon})$ due to two factors. On the one hand, the size of the central zone is $O(\sqrt{\varepsilon})$ and on the other hand, the growth of the amplitude of the cycle born at a Hopf-like bifurcation is linear with the parameter. Thus, for the limit cycle to enter the canard regime, it must first pass through the central region.
- *Supercritical case,* $m = -\sqrt{\varepsilon}$: System (4) is able to reproduce the dynamics in the smooth case with $k \leq 1$, that is, the existence of a family of stable canard cycles. By letting k increase, we find new scenarios that have not been reported in the smooth framework with cubic fast nullcline. In particular, when $k > 1$, we find situations where two saddle–node bifurcations of canard cycles take place, one of headless canards and another one of canards with head, see Fig. 9, panel (a). In this case, three canard limit cycles can coexist, see Fig. 10. In [17] authors present numerical evidences of the existence of the two saddle–nodes and hence, of the coexistence of the three canard cycles. It can be checked that systems (4) in the present manuscript and (2) in [17] are, locally, linear conjugated. Moreover, the values corresponding to the parameter sets II, III and IV appearing in Table 1 in [17], correspond with the parameter $k = 2.40$, $k = 2.89$ and $k = 11$, respectively, in our framework. Therefore, from Theorem 4.4, we can explain the unusual shape of the canard explosions appearing in Figure 6 and Figure 7A in [17].
- *Subcritical case,* $m = \sqrt{\varepsilon}$: In this case, system (4) is able to reproduce the dynamics in the smooth case, with the advantage that in the PWL case we can easier control the different behaviors that appear. In particular, we have proved the existence of saddle–node bifurcation of headless canards for $k < 1$, and of canards with head for $k > 1$, see Fig. 9, panel (b).
- Both in the supercritical and the subcritical scenario, the height of saddle–node canard cycles is a function of $\sqrt{\varepsilon}$, see function h^* in Propositions 5.3 and 5.6, as it is in the smooth context, see Theorem 3.6 in [3]. In fact, the existence of a non-hyperbolic canard cycle is derived in [3] after assuming the existence of a simple zero of the function $R(s)$. Nevertheless, in Propositions 5.3 and 5.6 we have already proved the existence of saddle–node canard cycles, by showing the existence of a zero of the function R_{3z} and R_{4z}.

Beyond the comparison with the results reported in [3], in Theorem 4.7 we have stated that, both in subcritical and supercritical cases, for every height between the smallest canard cycle and the relaxation oscillation cycle, there exist parameters k and ε such that a saddle–node canard limit cycle with this height exists.

Furthermore, note that in Fig. 9 we have represented the height of the saddle–node canard cycles versus the parameter k for a particular value of ε. The straight line corresponds with the height, h_M, of the canard orbit through the tangent point $\mathbf{p}_{LL}$, and coincides with the maximum height of a 3-zones, that it, the transitory saddle–node canard cycle. Hence, for $k_1 < k < k_2$ the saddle–node canard cycles predicted by function $h^*(k, \sqrt{\varepsilon}; m)$ do not correspond neither with 3-zones nor 4-zones saddle–node

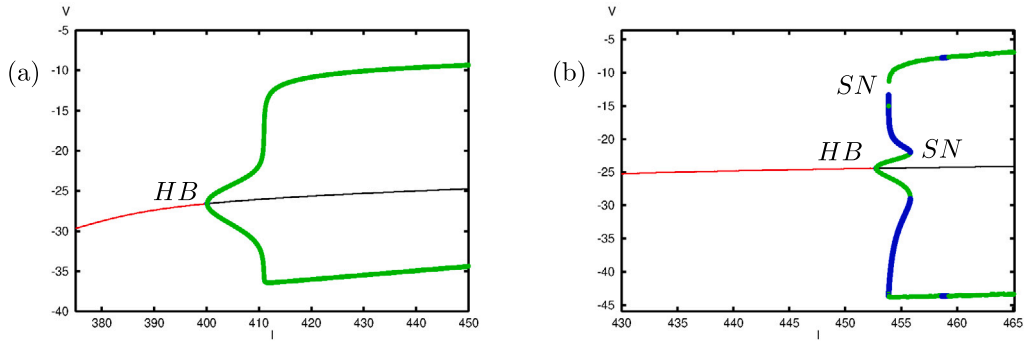

Fig. 11. Supercritical canard explosion in the Morris–Lecar neural model. HB stands for supercritical Hopf Bifurcation and SN for Saddle–Node bifurcation. (a) Canard explosion with ratio $k = 0.8514 < 1$ where all the canard cycles are hyperbolic and stable (green curve). (b) Canard explosion with ratio $k = 3.3540 > 1$ where two saddle–node cycles appear as collision of hyperbolic stable limit cycles (green part of the curve) and hyperbolic unstable limit cycles (blue part of the curve). (For interpretation of the references to color in this figure legend, the reader is referred to the web version of this article.)

canard cycles. It is clear that there must be a transition between both types of saddle–node canards and, as we have mentioned along the manuscript, such a transition cannot be obtained through the functions R_{3z} and R_{4z}, see (28) and (30), respectively. A similar situation happens in the smooth context, see [26], where slow divergence integral results to be not enough for the analysis of these transitory orbits. Although the results in the present article do not apply to transitory saddle–node canard cycles, from them, we can establish the following conjecture:

Conjecture 6.1. *For $\varepsilon = 0$, consider the transitory singular canard Γ, see [26], formed by the critical manifold in $[-1, 1]$ and the segment $\{(x, k) : x \in [-1, 1]\}$. There exist values of $\varepsilon > 0$ and k close to 1 such that corresponding system (4) exhibits one, two or three canard limit cycles in a neighborhood of Γ. Even more, the system also exhibits zero, one or two saddle–node canard cycles in a neighborhood of Γ.*

Finally, in the subcritical case, the existence of saddle–node bifurcation of headless canards for $k < 1$, and of canards with head for $k > 1$, leads us to come up with:

Conjecture 6.2. *System (4) in the subcritical case ($m = \sqrt{\varepsilon}$) possesses a saddle–node bifurcation of transitory canard cycles for $k = 1$.*

The use of this simpler family of slow–fast systems to reproduce canard dynamics brings us some information which could be interesting when revisiting the smooth context. In particular, the conditions $k < 1$ and $k > 1$ organizing the dynamics in the main results, suggest the importance of the ratio between the slopes of the fast nullcline in order to exhibit or not saddle–node canard cycles with head. Assuming this idea, we claim that saddle–node canard cycles with head can only appear when the average slope of the repelling branch of the critical manifold is greater than the average slope of the attracting branches of the critical manifold (in absolute value). As this is not the case in the Van der Pol system, it explains why only headless saddle–node canard cycles are possible in that system. To support the assertion about the linkage between the ratio of the slopes and the existence of saddle–node canard cycles, in Fig. 11 we show the behavior of the supercritical canard explosion in the Morris–Lecar neural model (37), see Appendix B for the definition of the elements involved. In particular, in panel (a) we show the supercritical canard explosion with ratio $k = 0.8514.... < 1$ where no saddle–node canard cycles are presented, as it is suggested by Theorem 4.4(a). On the contrary, in panel (b) we show the supercritical canard explosion with ratio $k = 3.3539... > 1$ where two saddle–node cycles appear, as it is also suggested by Theorem 4.4(b).

We finally point out that some quantitative information obtained in the manuscript could be relevant for applications. As example of such information we highlight the period of the canard cycles, see Lemma A.3, and the location of the saddle–node canards in terms of the parameter, see Propositions 5.2 and 5.5. Finally, the dependence between the height of a canard cycle and the bifurcation parameter a at which it appears has been approximated in the estimation $|a_N - a_S|$ appearing in Theorem 4.3. Note that, it can be observed that the slope of the explosion is different before and after the transitory canard.

CRediT authorship contribution statement

V. Carmona: Conceptualization, Formal analysis, Funding acquisition, Investigation, Methodology, Project administration, Resources, Software, Supervision, Validation, Visualization, Writing – original draft, Writing – review & editing. **S. Fernández-García:** Conceptualization, Formal analysis, Funding acquisition, Investigation, Methodology, Project administration, Resources, Software, Supervision, Validation, Visualization, Writing – original draft, Writing – review & editing. **A.E. Teruel:** Conceptualization, Formal analysis, Funding acquisition, Investigation, Methodology, Project administration, Resources, Software, Supervision, Validation, Visualization, Writing – original draft, Writing – review & editing.

Declaration of competing interest

The authors declare that they have no known competing financial interests or personal relationships that could have appeared to influence the work reported in this paper.

Data availability

No data was used for the research described in the article.

Acknowledgments

The three authors want to thank M. Desroches for introducing us into the problem and for his continuous support. They also thanks M. Krupa and S. Rodrigues for their fruitful conversations, and Jacobo Guerrero for his help in the analysis of the Morris–Lecar model.

First author is partially supported by Junta de Andalucía (Consejería de Economía, Conocimiento, Empresas y Universidad) projects TIC-0130, P12-FQM-1658, P20-01160 and US-1380740, and by the Ministerio de Ciencia, Innovación y Universidades (MCIU) projects PGC2018-096265-B-I00 and PID2021- 123200NB-I00. Second author is supported by Ministerio de Ciencia e Innovación, Spain through the project PID2021-123153OB-C21. Third author is supported by Ministerio de Economía y Competitividad through the project MTM2017-83568-P (AEI/ERDF, EU) and the project PID2020-118726GB-I00 funded by MCIN/AEI/10.13039/501100011033.

Appendix A. About Poincaré half-maps and times of flight

In this section we summarize the main technical results on piecewise linear dynamics that we use along the manuscript. In particular we provide approximations for the Poincaré half-map and for the time of flight of the solutions inside the regions of linearity.

Lemma A.1. *For $\varepsilon_0 > 0$ sufficiently small, set $\varepsilon < \varepsilon_0$, $a < \sqrt{\varepsilon}$, the values of x_r and x_s given in (14) and x_u given in (16). Let Γ_{x_0} be a limit cycle of system (4) having width $x_0 \in (x_r, a)$. It holds that:*

(a) If $x_0 \in (x_s, a)$ then Γ_{x_0} is under Hopf regime.
(b) If $x_0 \in (x_r, x_s)$ then Γ_{x_0} is under canard regime.
(c) If $x_0 \in (x_u, -1)$ then Γ_{x_0} is a canard cycle in transitory region.

Moreover, if $h = \Phi(x)$ is the function relating the width x of a limit cycle with its height h, see (11), then:

$$\begin{aligned} h_s &= \Phi(x_s) = \left(\frac{k}{|\ln(\varepsilon)|} - m\right)(\sqrt{\varepsilon} + a), \\ h_M &= \Phi(-1) = p_2, \\ h_u &= \Phi(x_u) = p_2 - \frac{1}{|\ln(\varepsilon)|}(1 + a), \\ h_r &= \Phi(x_r) = -(m + \lambda_L^s)(\sqrt{\varepsilon} + a), \end{aligned}$$

where $p_2 = -m\left(\sqrt{\varepsilon} + a\right) + k(1 - \sqrt{\varepsilon})$ is the second coordinate of $\mathbf{p}_{LL}$.

Proof. This proof is similar to that of Lemma 4.1 in [30] and is performed through the analysis of the divergence in a neighborhood of the repelling slow manifold.

In particular, for the first statement it suffices to adapt the proof of statement (a) of Lemma 4.1 in [30], taking into account that the trace in zone σ_L in now k, instead of 1, as we summarize below.

Let $\varphi(t)$ be a solution of system (4) such that $\varphi(t) \subset \sigma_L$ for $t \in (0, t_0)$ and $t_0 > 0$. By using the Krylov base $\{\mathbf{p}_L, \dot{\mathbf{p}}_L\}$, the solution can be parametrized by $\varphi(t) = u_1(t)\mathbf{p}_L + u_2(t)\dot{\mathbf{p}}_L$. Following Theorem 5 in [33], the function $H_L(u_1, u_2) = |u_1 + \lambda_L^s u_2|^{\lambda_L^q} |u_1 + \lambda_L^q u_2|^{-\lambda_L^s}$ is constant over the coordinates $(u_1(t), u_2(t))$ with $t \in (0, t_0)$, and it is called a first integral for system (4) related to the Krylov base $\{\mathbf{p}_L, \dot{\mathbf{p}}_L\}$. Therefore, the transition map from points on the switching line $\{x = -\sqrt{\varepsilon}\}$ to itself, i.e., from points $\mathbf{p}_L - u\dot{\mathbf{p}}_L$ to points $\mathbf{p}_L + v\dot{\mathbf{p}}_L$, is given by $H_L(1, -u) = H_L(1, v)$.

Thus, following the same steps that in the proof of statement (a) of Lemma 4.1 in [30], we can deduce that the transition map from points in $\{x = -\sqrt{\varepsilon}\}$ into points in the $x-$nullcline in zone σ_L is given by,

$$H_L(1, -u_s(\varepsilon)) = H_L(\gamma, 0). \tag{34}$$

Moreover, $H_L(1, -u_s(\varepsilon)) = 1 + \frac{1}{|\ln(\varepsilon)|}$. Also $H_L(\gamma, 0) = \gamma^{\lambda_L^q - \lambda_L^s}$ which can be approximated at first order by γ^k. Taking this into account, from expression (34) we find that $\gamma^k \approx 1 + \frac{1}{|\ln(\varepsilon)|}$. Thus, x_s can be computed as the first coordinate of the point $\mathbf{e}_L + \gamma(\mathbf{p}_L - \mathbf{e}_L)$, from which we obtain the second expression in (14).

Let us proceed now to the computation of x_r. Following the same steps as in the proof of statement (b) in Lemma 4.1 in [30], we get that,

$$r^{\lambda_L^q-\lambda_L^s}F(-v)=r^{\lambda_L^q-\lambda_L^s}\frac{1-v\lambda_L^s}{1-u_r\lambda_L^s}\approx r^k\frac{1-v\lambda_L^s}{1-u_r\lambda_L^s},$$

and we conclude that $v_r(\varepsilon)=\frac{1}{\lambda_L^s}\left(1-\varepsilon^{1/k}\left(1+\frac{1}{|\ln(\varepsilon)|}\right)\right)$.

Now, by using the Krylov base $\{\mathbf{p}_{LL},\dot{\mathbf{p}}_{LL}\}$, the solution can be parametrized by $\varphi(t)=u_1(t)\mathbf{p}_{LL}+u_2(t)\dot{\mathbf{p}}_{LL}$. Following again Theorem 5 in [33], function $H_{LL}(u_1,u_2)=|u_1+\lambda_{LL}^s u_2|^{\lambda_{LL}^q}|u_1+\lambda_{LL}^q u_2|^{-\lambda_{LL}^s}$ is constant over the coordinates $(u_1(t),u_2(t))$ with $t\in(0,t_0)$, and it is called a first integral for system (4) related to the Krylov base $\{\mathbf{p}_{LL},\dot{\mathbf{p}}_{LL}\}$. Therefore, the transition map from points on the switching line $\{x=-1\}$ to itself, i.e., from points $\mathbf{p}_{LL}-u\dot{\mathbf{p}}_{LL}$ to points $\mathbf{p}_{LL}+v\dot{\mathbf{p}}_{LL}$, is given by $H_{LL}(1,-u)=H_{LL}(1,v)$, and we can deduce that the transition map from points in $\{x=-1\}$ into points in the $x-$nullcline in zone σ_{LL} is given by,

$$H_{LL}(1,-v_r(\varepsilon))=H_{LL}(\gamma,0). \tag{35}$$

Also, $H_{LL}(\gamma,0)=\gamma^{\lambda_{LL}^q-\lambda_{LL}^s}$ which can be approximated at first order by γ^{-1}. Taking this into account, from expression (35) we find that $\gamma\approx 2/(1+v_r)^\epsilon$. Thus, x_r can be computed as the first coordinate of the point $\mathbf{e}_{LL}+\gamma(\mathbf{p}_{LL}-\mathbf{e}_{LL})$, from which we obtain the first expression in (14).

Finally, we deal with the computation of x_u. As it can be seen in Fig. 7, this value corresponds to the first component of the intersection with the $x-$nullcline of the orbit from an initial point in the separation line $x=-1$, such that the following intersection with this separation line is below and exponentially close to $\mathbf{q}_1^{LL}$.

Again, by using the Krylov base $\{\mathbf{p}_{LL},\dot{\mathbf{p}}_{LL}\}$, we know that the transition map from points on the switching line $\{x=-1\}$ to itself, is given by $H_{LL}(1,-u)=H_{LL}(1,v)$, and we can deduce that the transition map from points in the $x-$nullcline in zone σ_{LL} into points in $\{x=-1\}$ is given by,

$$H_{LL}(\gamma,0)=H_{LL}(1,v_u(\varepsilon)). \tag{36}$$

Taking into account that, $H_{LL}(\gamma,0)=\gamma^{\lambda_{LL}^q-\lambda_{LL}^s}$, which can be approximated at first order by γ^{-1}, we find from expression (36) that $\gamma\approx 1+1/|\ln\varepsilon|-\varepsilon$. Thus, x_u can be computed as the first coordinate of the point $\mathbf{e}_{LL}+\gamma(\mathbf{p}_{LL}-\mathbf{e}_{LL})$, from which we obtain the first expression in (16).

Now we deal with the computations of the height h_s, the reminder values follow in a similar way. Since u_s is known, from expression $H_L(1,-u_s)=H_L(1,v_s)$, we obtain the value

$$v_s=\frac{1}{\lambda_L^s|\ln(\varepsilon)|}=\frac{k}{\varepsilon|\ln(\varepsilon)|}.$$

Therefore, h_s can be computed as the second coordinate of the point $\mathbf{p}_L+v_s\dot{\mathbf{p}}_L$, given the expression provided in the lemma. □

Lemma A.2. *For $\varepsilon_0>0$ fixed and small enough, and $\varepsilon\in(0,\varepsilon_0)$ it follows that*

$$\Pi_L^{-1}\left(\begin{pmatrix}-\sqrt{\varepsilon}\\ h\end{pmatrix}\right)-\mathbf{q}_0^L=\begin{pmatrix}0\\ (h+O(\varepsilon))e^{-\frac{kh}{\varepsilon(\sqrt{\varepsilon}-a)}}\end{pmatrix},\quad \text{for } h>h_s,$$

$$\Pi_R\left(\begin{pmatrix}\sqrt{\varepsilon}\\ h\end{pmatrix}\right)-\mathbf{q}_1^R=\begin{pmatrix}0\\ (h+O(\varepsilon))e^{-\frac{h}{\varepsilon(\sqrt{\varepsilon}-a)}}\end{pmatrix},\quad \text{for } h>h_R:=\left(m+\frac{1}{|\ln(\varepsilon)|}\right)(\sqrt{\varepsilon}-a),$$

$$\mathbf{q}_1^{LL}-\Pi_{LL}\left(\begin{pmatrix}-1\\ h\end{pmatrix}\right)=\begin{pmatrix}0\\ (k-h+O(\varepsilon))e^{-\frac{k(k-h)}{\varepsilon(1+a)}}\end{pmatrix},\quad \text{for } h<h_u,$$

$$\mathbf{q}_0^L-\Pi_{Ld}^{-1}\left(\begin{pmatrix}-1\\ h\end{pmatrix}\right)=\begin{pmatrix}0\\ (k-h+O(\varepsilon))e^{-\frac{k}{\varepsilon}\ln\left(\frac{1+a}{a+\sqrt{\varepsilon}}\right)}\end{pmatrix},\quad \text{for } h\in(h_r,p_2),$$

where h_s,h_u and h_r are provided in Lemma A.1, and $p_2=k(1-\sqrt{\varepsilon})-m(\sqrt{\varepsilon}+a)$ is the second coordinate of the point $\mathbf{p}_{LL}$.

Proof. Next, we compute the expressions of the Poincaré half-maps Π_R and Π_{Ld}, the remainder expressions in the lemma follows in a similar way.

Following Chapter 3 in [36], the coordinates u and v of the points $\mathbf{p}$ and $\Pi_R(\mathbf{p})$ in the Krylov base $\{\mathbf{p}_R,\dot{\mathbf{p}}_R\}$, that is, $\mathbf{p}=\mathbf{p}_R-u\dot{\mathbf{p}}_R$ and $\Pi_R(\mathbf{p})=\mathbf{p}_R+v\dot{\mathbf{p}}_R$, are invariant through translations and linear transformation. Therefore, u and v satisfy that $v\in\left(0,-\frac{1}{\lambda_R^q}\right)$ and

$$\left(\frac{1+v\lambda_R^s}{1-u\lambda_R^s}\right)^{\frac{\lambda_R^q}{\lambda_R^s}}=\frac{1+v\lambda_R^q}{1-u\lambda_R^q},$$

where λ_R^s and λ_R^q are the slow and the fast eigenvalues of the matrix A_R. For ϵ small enough, λ_R^s tends to zero and hence, taking the limit of the left side term in the previous identity as λ_R^s tends to zero, we obtain that v can be implicitly approximated by

$$v = \frac{1}{\lambda_R^q}\left(-1 + (1 - u\lambda_R^q)e^{\lambda_R^q(u+v)}\right).$$

Since the u-coordinate of $\mathbf{p} = (\sqrt{\varepsilon}, h)^T$ in the Krylov base is

$$u = \frac{h - m(\sqrt{\varepsilon} - a)}{\varepsilon(\sqrt{\varepsilon} - a)} > 0,$$

we conclude that

$$\begin{aligned}
\Pi_R(\mathbf{p}) &= \mathbf{p}_R + \frac{1}{\lambda_R^q}\left(-1 + (1 - u\lambda_R^q)e^{\lambda_R^q(u+v)}\right)\dot{\mathbf{p}}_R \\
&= \begin{pmatrix} \sqrt{\varepsilon} \\ (m + \lambda_R^s)(\sqrt{\varepsilon} - a) - \left(\lambda_R^s(\sqrt{\varepsilon} - a) - u\varepsilon(\sqrt{\varepsilon - a})\right)e^{\lambda_R^q(u+v)} \end{pmatrix} \\
&= \begin{pmatrix} \sqrt{\varepsilon} \\ (m + \lambda_R^s)(\sqrt{\varepsilon} - a) - \left((m + \lambda_R^s)(\sqrt{\varepsilon} - a) - h\right)e^{\lambda_R^q(v + \frac{h - m(\sqrt{\varepsilon}-a)}{\varepsilon(\sqrt{\varepsilon}-a)})} \end{pmatrix} \\
&= \mathbf{q}_1^R + \begin{pmatrix} 0 \\ \left(h - (m + \lambda_R^s)(\sqrt{\varepsilon} - a)\right)e^{\lambda_R^q v + \frac{h - m(\sqrt{\varepsilon}-a)}{\lambda_R^s(\sqrt{\varepsilon}-a)}} \end{pmatrix}.
\end{aligned}$$

Taking into account that $-1 < \lambda_R^q v < 0$, the exponent in the previous expression can be approximated by $\frac{h}{\lambda_R^s(\sqrt{\varepsilon}-a)}$, provided that,

$$\frac{h - m(\sqrt{\varepsilon} - a)}{\lambda_R^s(\sqrt{\varepsilon} - a)} < -\frac{1}{\varepsilon|\ln(\varepsilon)|}.$$

From this we conclude that $h > \left(m + \frac{1}{|\ln(\varepsilon)|}\right)(\sqrt{\varepsilon} - a)$, what finishes the proof of the second expression of the lemma.

Consider now the transformation Π_{Ld}, from points of the form $\mathbf{p}_L - u\dot{\mathbf{p}}_L$ to points of the form $\mathbf{p}_{LL} - v\dot{\mathbf{p}}_{LL}$. Even when the relationship between the coordinates u and v of these points is not explicitly computed in [36], we can use the same arguments than there to obtain that $v \in \left(0, \frac{1}{\lambda_L^s}\right)$ and

$$\left(\frac{1 - v\lambda_L^s}{1 - u\lambda_L^s}\right)^{\frac{\lambda_L^q}{\lambda_L^s}} = r^{1 - \frac{\lambda_L^q}{\lambda_L^s}}\left(\frac{1 - v\lambda_L^q}{1 - u\lambda_L^q}\right),$$

where $r = \frac{1+a}{\sqrt{\epsilon}+a}$ satisfies that $\mathbf{p}_{LL} - \mathbf{e}_L = r(\mathbf{p}_L - \mathbf{e}_L)$. Taking the limit of the left side term in the previous identity as λ_L^s tends to zero, we obtain a new implicit relation between the coordinates u and v given by

$$u = \frac{1}{\lambda_L^q}\left(1 - r(1 - v\lambda_L^q)e^{-\frac{\lambda_L^q}{\lambda_L^s}\ln(r) + \lambda_L^q(v-u)}\right).$$

Since the v coordinate of a point $(-1, h) = \mathbf{p}_{LL} - v\dot{\mathbf{p}}_{LL}$ satisfies that

$$v = \frac{k(1 - \sqrt{\varepsilon}) - m(\sqrt{\varepsilon} + a) - h}{\varepsilon(1 + a)} \in \left(0, \frac{1}{\lambda_L^s}\right),$$

it follows that

$$k(1 - \sqrt{\varepsilon}) - m(\sqrt{\varepsilon} + a) - \lambda_L^q(1 + a) < h < k(1 - \sqrt{\varepsilon}) - m(\sqrt{\varepsilon} + a),$$

and therefore, the preimage by Π_{Ld} of the point $(-1, h)$ is

$$\mathbf{p}_L - u\dot{\mathbf{p}}_L = \mathbf{q}_0^L + \begin{pmatrix} 0 \\ \left((1 + a)\lambda_L^s + m(a + \sqrt{\varepsilon}) - k(1 - \sqrt{\varepsilon}) + h\right)e^{-1 - \frac{\lambda_L^q(1+a)\ln(r) - k(1-\sqrt{\varepsilon}) + m(\sqrt{\varepsilon}+a) + h}{\lambda_L^s(1+a)}} \end{pmatrix}.$$

For ε small enough previous expression can be rewritten as

$$\mathbf{p}_L - u\dot{\mathbf{p}}_L = \mathbf{q}_0^L + \begin{pmatrix} 0 \\ \left((m+k)(a+\sqrt{\varepsilon}) - \lambda_L^q(1+a) + h\right) e^{-\frac{k}{\varepsilon}\ln\left(\frac{1+a}{\sqrt{\varepsilon}+a}\right)} \end{pmatrix}.$$

The lemma for Π_{Ld} follows by considering ε small enough. □

Let $\tau_R(h)$ be the time of flight of the solution between the points $(\sqrt{\varepsilon}, h)^T$ and $\Pi_R(\sqrt{\varepsilon}, h)$, let $\tau_L(h)$ be the time of flight between $(-\sqrt{\varepsilon}, h)^T$ and $\Pi_L(-\sqrt{\varepsilon}, h)$, let $\tau_{LL}(h)$ be the time of flight between $(-1, h)^T$ and $\Pi_{LL}(-1, h)$, let $\tau_{Ld}(h)$ be the time of flight between $(-\sqrt{\varepsilon}, h)^T$ and $\Pi_{Ld}(-\sqrt{\varepsilon}, h)$ and let τ_{RR} be the time of flight between $\mathbf{q}_0^{RR}$ and $\mathbf{q}_1^R$, see Fig. 2, that is, $\tau_{RR} = \tau_R(h_0)$ where h_0 is the second coordinate of $\mathbf{q}_1^{LL}$. In the following lemma, we provide such times of flight.

Lemma A.3. *For $\varepsilon > 0$ fixed and small enough it follows that*

$$\begin{aligned}
\tau_R(h) &= -\frac{1}{\lambda_R^s}\ln\left(1 + \frac{(m+\lambda_R^s)(\sqrt{\varepsilon}-a) - h}{(\lambda_R^q - \lambda_R^s)(\sqrt{\varepsilon}-a)}\right),\\
\tau_L(h) &= \frac{1}{\lambda_L^s}\ln\left(1 + \frac{h + (m+\lambda_L^s)(\sqrt{\varepsilon}+a)}{(\lambda_L^q - \lambda_L^s)(\sqrt{\varepsilon}+a)}\right),\\
\tau_{Ld}(h) &= \frac{1}{\lambda_L^s}\ln\left(1 + \frac{h + m(\sqrt{\varepsilon}+a) + \lambda_L^s(2\sqrt{\varepsilon}+a-1)}{(\lambda_L^q - \lambda_L^s)(\sqrt{\varepsilon}+a)}\right),\\
\tau_{LL}(h) &= -\frac{1}{\lambda_{LL}^s}\ln\left(1 + \frac{h + m(\sqrt{\varepsilon}+a) + k(\sqrt{\varepsilon}-1) + \lambda_{LL}^s(1+a)}{(\lambda_{LL}^q - \lambda_{LL}^s)(1+a)}\right),\\
\tau_{RR} &= -\frac{1}{\lambda_R^s}\ln\left(1 + \frac{\lambda_R^s(\sqrt{\varepsilon}-a) + \lambda_{LL}^s(1+a) + k(\sqrt{\varepsilon}-1) + 2m\sqrt{\varepsilon}}{(\lambda_R^q - \lambda_R^s)(\sqrt{\varepsilon}-a)}\right).
\end{aligned}$$

Proof. Consider a point $\mathbf{p} = (\sqrt{\varepsilon}, h)^T$ and its image by the Poincaré map $\Pi_R(\mathbf{p})$. From Lemma A.2, since ε is small enough, we can substitute the point $\Pi_R(\mathbf{p})$ by the exponentially close point $\mathbf{q}_1^R$. In an equivalent way, we approximately compute the time $\tau_R(h)$ as the time of flight of the solution for traveling from $\mathbf{p}$ to $\mathbf{q}_1^R$. To do that, we project the point $\mathbf{p}$ onto the point $\mathbf{p}_s$ contained in the slow manifold μ_R, see (7), by following the fast eigenvector, $\mathbf{v}_R^q$. The point $\mathbf{p}_s$ is obtained by solving with respect the unknowns $r_s, r_q \in \mathbb{R}^+$ the linear system of equations

$$\mathbf{p}_s = \mathbf{p} - r_q\mathbf{v}_R^q = \mathbf{e}_R - r_s\mathbf{v}_R^s.$$

We conclude that

$$r_s = \frac{(\sqrt{\varepsilon}-a)(m-1-\lambda_R^s) - h}{\lambda_R^s(\lambda_R^s - \lambda_R^q)} = \frac{(\sqrt{\varepsilon}-a)(m+\lambda_R^q) - h}{\lambda_R^s(\lambda_R^s - \lambda_R^q)}.$$

Then, we compute $\tau_R(h)$ as the time of flight of the solution to travel from the projected point $\mathbf{p}_s$ to $\mathbf{q}_1^R$, that is,

$$e^{\lambda_R^s\tau_R(h)} = \frac{\|\mathbf{q}_1^R - \mathbf{e}_R\|}{\|\mathbf{p}_s - \mathbf{e}_R\|} = \frac{\frac{a-\sqrt{\varepsilon}}{\lambda_R^s}\|\mathbf{v}_R^s\|}{r_s\|\mathbf{v}_R^s\|} = \frac{(\sqrt{\varepsilon}-a)(\lambda_R^q - \lambda_R^s)}{(\sqrt{\varepsilon}-a)(m+\lambda_R^q) - h}.$$

The lemma follows by isolating $\tau_R(h)$. The remainder functions are computed by following similar arguments. □

Appendix B. Morris–lecar neural model

In this section we introduce the Morris–Lecar neural model [37]

$$\begin{cases} C\dot{V} = I - g_L(V - E_L) - g_{Na}m_\infty(V)(V - E_{Na}) - g_k n(V - E_K), \\ \dot{n} = \dfrac{n_\infty(V) - n}{\tau_n(V)} \end{cases} \tag{37}$$

where

$$m_\infty(V) = \frac{1}{1 + e^{\frac{V_m - V}{k_m}}}, \quad n_\infty(V) = \frac{1}{1 + e^{\frac{V_n - V}{k_n}}}, \quad \tau_n(V) = \tau_n.$$

We also provide the values of the parameters allowing for the canard explosions in Fig. 11. In particular, for the panel (a) the used parameters are: $C = 1$, $E_{Na} = 40$, $E_K = -70$, $E_L = -78$, $g_{Na} = 5$, $g_k = 5$, $g_L = 8$, $k_m = 3$, $V_m = -20$, $k_n = 1.188$, $V_n = -24$ and $\tau_n = 1$. For these parameters, the local minimum and maximum of the $V-$nullcline are located at the points $(-26.6758, 0.3223)$ and $(-16.2482, 0.6344)$, respectively. Moreover, for computing the ratio of the slopes we also consider the point $(-35.2413, 0.6234)$ on the

$V-$nullcline. Therefore, the slope of the left attracting branch of the slow manifold is given by $s_a = \frac{0.6234-0.3223}{35.2413-26.6758} = 0.0352$, and the slope of the repelling branch of the slow manifold is given by $s_u = \frac{0.6344-0.3223}{26.6758-16.2482} = 0.0299$. The ratio between the slopes are $k = \frac{s_u}{s_a} = \frac{0.0299}{0.0352} = 0.8514$.

For the panel (b) the used parameters are: $C = 1$, $E_{Na} = 60$, $E_K = -90$, $E_L = -78$, $g_{Na} = 7$, $g_k = 10$, $g_L = 8$, $k_m = 1.28$, $V_m = -20$, $k_n = 0.9$, $V_n = -22$ and $\tau_n = 0.2$. For these parameters, the local minimum and maximum of the $V-$nullcline are located at the points $(-24,5655, 0.0762)$ and $(-16.4965, 0.6454)$, respectively. Moreover, for computing the ratio of the slopes we also consider the point $(-50.7586, 0.6271)$ on the $V-$nullcline. Therefore, the slope of the left attracting branch of the slow manifold is given by $s_a = \frac{0.6271-0.0762}{50.7586-24.5655} = 0.0210$, and the slope of the repelling branch of the slow manifold is given by $s_u = \frac{0.6454-0.0762}{24.5655-16.4965} = 0.0705$. The ratio between the slopes are then $k = \frac{s_u}{s_a} = \frac{0.0705}{0.0210} = 3.3540$.

References

[1] F. Dumortier, R. Roussarie, Canard Cycles and Center Manifolds, Vol. 121, AMS, Providence (RI), 1996.
[2] W. Eckhaus, Standard chase on French Ducks, Lecture Notes in Math. 985 (1983) 449–494.
[3] M. Krupa, P. Szmolyan, Relaxation oscillation and canard explosion, J. Differential Equations 174 (2001) 312–368.
[4] E. Benoit, J.-L. Callot, F. Diener, et al., Chasse au canard, Collect. Math. 32 (1–2) (1981) 37–119.
[5] P. De Maesschalck, F. Dumortier, R. Roussarie, Canard Cycles: From Birth to Transition, in: A Series of Modern Surveys in Mathematics, Springer International Publishing, 2021.
[6] R. FitzHugh, Impulses and physiological states in theoretical models of nerve membrane, Biophys. J. 1 (1961) 445–466.
[7] E.M. Izhikevich, Dynamical Systems in Neuroscience: The Geometry of Excitability and Bursting, The MIT Press Cambridge, Massachusetts London, England, 2007.
[8] J. Nagumo, S. Arimoto, S. Yoshizawa, An active pulse transmission line simulating nerve axon, Proc. IRE 50 (1962) 2061–2070.
[9] M. Wechselberger, Geometric Singular Perturbation Theory beyond the Standard Form, Springer, 2020.
[10] N. Fenichel, Geometric singular perturbation theory for ordinary differential equations, J. Differential Equations 31 (1) (1979) 53–98.
[11] M. Krupa, P. Szmolyan, Extending geometric singular perturbation theory to nonhyperbolic points-fold and canard points in two dimensions, SIAM J. Math. Anal. 33 (2) (2001) 286–314.
[12] P. Toniol Cardin, Relaxation oscillation in planar discontinuous piecewise smooth fast–slow systems, Chaos 32 (1) (2022).
[13] A. Roberts, Canard explosion and relaxation oscillation in planar, piecewise-smooth, continuous systems, SIAM J. Appl. Dyn. Syst. 15 (2016) 608–624.
[14] A. Roberts, P. Glendinning, Canard-like phenomena in piecewise-smooth Van der Pol systems, Chaos 24 (2014) 023138.
[15] M. Desroches, S. Fernández-García, M. Krupa, Canards in a minimal piecewise-linear square-wave burster, Chaos 26 (2016).
[16] M. Desroches, A. Guillamon, E. Ponce, R. Prohens, S. Rodrigues, A.E. Teruel, Canards, Folded nodes and mixed-mode oscillations in piecewise-linear slow-fast systems, SIAM Rev. 58 (4) (2016) 653–691.
[17] H.G. Rotstein, S. Coombes, A.M. Gheorghe, Canard-like explosion of limit cycles in two dimensional piecewise-linear models of FitzHugh–Nagumo type, SIAM J. Appl. Dyn. Syst. 11 (1) (2012) 135–180.
[18] M. Desroches, S. Fernández-García, M. Krupa, R. Prohens, A.E. Teruel, Piecewise-linear (PWL) canard dynamics: Simplifying singular perturbation theory in the canard regime using piecewise-linear systems, in: Nonlinear Systems, Vol. 1 : Mathematical Theory and Computational Methods, Springer, 2018.
[19] M. Desroches, E. Freire, S.J. Hogan, E. Ponce, P. Thota, Canards in piecewise-linear systems: explosions and super-explosions, Proc. R. Soc. Lond. Ser. A Math. Phys. Eng. Sci. 469 (2154) (2013) 20120603.
[20] S. Fernández-García, M. Desroches, M. Krupa, A.E. Teruel, Canard solutions in planar piecewise linear systems with three zones, Dynam. Syst. 31 (2) (2016) 173–197.
[21] K.R.T. Jones Christopher, Geometric singular perturbation theory, in: Dynamical Systems: Lectures Given at the 2nd Session of the Centro Internazionale Matematico Estivo (C.I.M.E.) Held in Montecatini Terme, Italy, June 13–22, 1994, Springer Berlin Heidelberg, 1995.
[22] B. Braaksma, Singular Hopf bifurcation in systems with fast and slow variables, J. Nonlinear Sci. 8 (5) (1998) 457–490.
[23] J. Guckenheimer, Singular Hopf bifurcation in systems with two slow variables, SIAM J. Appl. Dyn. Syst. 7 (4) (2008) 1355–1377.
[24] F. Dumortier, Slow divergence integral and balanced canard solutions, Qual. Theory Dyn. Syst. 10 (1) (2011) 65–85.
[25] R. Prohens, A.E. Teruel, C. Vich, Slow–fast n-dimensional piecewise linear differential systems, J. Differential Equations 260 (2016) 1865–1892.
[26] P. De Maesschalck, F. Dumortier, R. Roussarie, Canard cycle transition at a slow-fast passage through a jump point, C. R. Math. 352 (2014) 317–320.
[27] C. Chicone, Bifurcations of nonlinear oscillations and frequency entrainment near resonance, SIAM J. Math. Anal. 23 (6) (1992) 1577–1608.
[28] E. Freire, E. Ponce, F. Rodrigo, F. Torres, Bifurcation sets of continuous piecewise linear systems with two zones, Internat. J. Bifur. Chaos Appl. Sci. Engrg. 8 (11) (1998) 2073–2097.
[29] D.J.W. Simpson, Twenty Hopf-like bifurcations in piecewise-smooth dynamical systems, Phys. Rep. (2019) 146120887.
[30] V. Carmona, S. Fernández-García, A.E. Teruel, Birth, transition and maturation of canard cycles in a piecewise linear system with a flat slow manifold, Physica D 443 (2023) 133566.
[31] D.J.W. Simpson, A compendium of Hopf-like bifurcations in piecewise-smooth dynamical systems, Phys. Lett. A 382 (2018) 2439–2444.
[32] S. Lang, Calculus of Several Variables, third ed., in: Undergraduate Texts in Mathematics, Springer, 1987.
[33] J. Llibre, E. Nuñez, A.E. Teruel, Limit cycles for planar piecewise linear differential systems via first integrals, Qual. Theory Dyn. Syst. 3 (2002) 29–50.
[34] Y.A. Kuznetsov, Elements of Applied Bifurcation Theory, third ed., Springer, 2004.
[35] L. Perko, Differential Equations and Dynamical Systems, in: Springer-Verlag, 2001.
[36] J. Llibre, A.E. Teruel, Introduction to the Qualitative Theory of Differential Systems: Planar, Symmetric and Continuous Piecewise Linear Systems, in: Birkhäuser Advanced Texts Basler Lehrbücher, Springer Basel, Basel, 2014.
[37] C. Morris, H. Lecar, Voltage oscillations in the barnacle giant muscle fiber, Biophys. J. 35 (1981) 193–213.